Unique pathological tau conformers from Alzheimer's brains transmit tau pathology in nontransgenic mice

Jing L. Guo, Sneha Narasimhan, Lakshmi Changolkar, Zhuohao He, Anna Stieber, Bin Zhang, Ronald J. Gathagan, Michiyo Iba, Jennifer D. McBride, John Q. Trojanowski, and Virginia M.Y. Lee

Department of Pathology and Laboratory Medicine, Institute on Aging and Center for Neurodegenerative Disease Research, University of Pennsylvania School of Medicine, Philadelphia, PA 19104

Filamentous tau aggregates are hallmark lesions in numerous neurodegenerative diseases, including Alzheimer's disease (AD). Cell culture and animal studies showed that tau fibrils can undergo cell-to-cell transmission and seed aggregation of soluble tau, but this phenomenon was only robustly demonstrated in models overexpressing tau. In this study, we found that intracerebral inoculation of tau fibrils purified from AD brains (AD-tau), but not synthetic tau fibrils, resulted in the formation of abundant tau inclusions in anatomically connected brain regions in nontransgenic mice. Recombinant human tau seeded by AD-tau revealed unique conformational features that are distinct from synthetic tau fibrils, which could underlie the differential potency in seeding physiological levels of tau to aggregate. Therefore, our study establishes a mouse model of sporadic tauopathies and points to important differences between tau fibrils that are generated artificially and authentic ones that develop in AD brains.

The Journal of Experimental Medicine

INTRODUCTION

Neurofibrillary tangles (NFTs), the cytoplasmic filamentous accumulations of tau protein, are hallmark lesions of Alzheimer's disease (AD) and other age-related neurodegenerative diseases, collectively termed tauopathies (Lee et al., 2001). Tau is a microtubule (MT)-associated protein predominantly expressed in neuronal axons with a primary function of promoting assembly and stability of MTs (Weingarten et al., 1975; Cleveland et al., 1977b). The adult brain expresses six isoforms of tau with three or four MT-binding repeats (3R or 4R) that bind the inner surface of MTs and zero to two acidic N-terminal inserts (0N, 1N, or 2N) that project away from MTs (Goedert et al., 1989). Although normally a highly soluble protein without well-defined secondary or tertiary structures, tau assembles into β sheet–rich insoluble amyloid fibrils, commonly known as paired helical filaments (PHFs), to form NFTs in AD brains (Cleveland et al., 1977a; Lee et al., 1991; Mandelkow et al., 2007). These pathological tau aggregates are believed to play critical roles in neuronal dysfunction and neurodegeneration.

Increasing evidence suggests filamentous tau aggregates are self-perpetuating entities capable of undergoing cell-to-cell transmission, whereby extracellular tau fibrils enter cells through endocytosis and seed the recruitment of soluble tau into growing aggregates, some of which get released and taken up by healthy cells to induce another cycle of seeded fibrillization (Frost et al., 2009; Guo and Lee, 2011, 2013; Kfoury et al., 2012; Wu et al., 2013). Importantly, a single intracerebral inoculation of synthetic tau fibrils assembled from recombinant tau (rTau) protein or tau aggregate–containing brain homogenates into transgenic (Tg) mice overexpressing tau was shown to induce and propagate NFT-like tau pathology to anatomically connected brain regions (Clavaguera et al., 2009, 2013; Iba et al., 2013). This connectome-dependent transmission of pathological tau is proposed to underlie the stereotypical spatiotemporal progression of NFTs in AD brains (Guo and Lee, 2014; Walker and Jucker, 2015).

Most studies demonstrating transmissibility of tau aggregates were conducted in the presence of tau overexpression, often coupled to mutations that further enhance the fibrillization propensity of tau. However, increased tau expression is not a cause of AD or other tauopathies, and tau mutations are only found in rare cases of frontotemporal dementia. Hence, cellular and animal models that recapitulate the vast majority of tauopathies, which are sporadic in nature, remain to be developed. Although we and others demonstrated that it is possible to trigger aggregation of non-overexpressed WT tau in cultured neurons and in mice (Lasagna-Reeves et al., 2012; Clavaguera et al., 2013; Guo and Lee, 2013), the limited extent of induced pathology was far from sufficient to model cell-to-cell transmission as the underlying basis for progression of sporadic tauopathies.

Because of its high solubility, efficient fibrillization of tau in vitro can only be achieved in the presence of polyan-

Correspondence to Virginia M.Y. Lee: vmylee@upenn.edu

Abbreviations used: AD, Alzheimer's disease; BCA, bicinchoninic acid; CBD, corticobasal degeneration; DPBS, Dulbecco's PBS; DTT, dithiothreitol; EM, electron microscopy; HA, hemagglutinin; Hep-T40, heparin-induced T40; IHC, immunohistochemistry; MT, microtubule; NFT, neurofibrillary tangles; PFA, paraformaldehyde; PHF, paired helical filament; p.i., postinjection; PSP, progressive supranuclear palsy; RIPA, radioimmunoprecipitation assay; rTau, recombinant tau; Tg, transgenic.

The Rockefeller University Press $30.00
J. Exp. Med. 2016 Vol. 213 No. 12 2635–2654
https://doi.org/10.1084/jem.20160833

ionic cofactors, with heparin being the most commonly used agent (Goedert et al., 1996; Kampers et al., 1996; Chirita et al., 2003). Heparin-induced tau fibrils were thought to resemble AD PHFs and were widely used to investigate the structural mechanism of PHF assembly (Friedhoff et al., 1998; Mandelkow et al., 2007; Siddiqua and Margittai, 2010). Although these fibrils can seed robust tau aggregation in cultured cells and mouse brains overexpressing human mutant tau, only low levels of pathology were induced in primary neurons derived from non-Tg mice (Guo and Lee, 2013). Based on studies suggesting conformational diversity of tau aggregates (Clavaguera et al., 2013; Sanders et al., 2014), we hypothesize different conformational variants of tau fibrils exist, with differential potency to seed the fibrillization of physiological levels of WT tau.

RESULTS

Generating different variants of tau fibrils with distinct seeding patterns in non-Tg neurons

In an attempt to generate more potent tau seeds than heparin-induced tau fibrils, we performed repetitive self-seeded fibrillization of recombinant T40 (4R2N human tau) in vitro, a method we previously used to generate different conformational variants of α-synuclein (α-syn) fibrils with differential seeding activities (Guo et al., 2013). As expected from the high solubility of tau, de novo fibrillization of T40 (passage 1 [P1]) without any cofactors did not result in any appreciable insoluble tau (Fig. 1 A). Interestingly, continual seeding of T40 monomers with fibrillization mixture from the previous passage (see the rTau purification and in vitro fibrillization section of Materials and methods) led to progressive increase in the percentage of pelletable tau and successful formation of fibrils confirmed by negative staining electron microscopy (EM; Fig. 1, A–C).

We also developed a simple protocol to purify tau PHFs from AD brains using differential centrifugation of the sarkosyl-insoluble brain fraction (Fig. 1, D–F; and Table S1). Compared with the traditional purification method using sucrose gradient (Lee et al., 1999), our new protocol resulted in much higher yields of PHF-tau (15–30 μg tau per gram of gray matter using our new protocol vs. 1–5 μg tau per gram of gray matter using the traditional protocol) with remarkable purity, whereby the dominant protein bands revealed by silver staining at 50–75 kD matched immunoreactivities of different anti-tau antibodies, and negative staining EM showed the presence of abundant filaments (Fig. 1, G and H). Further characterizations using bicinchoninic acid (BCA) assay and sandwich ELISA showed 10–28% purity of our AD PHF preparations (hereafter referred to as AD-tau), which contain minimal Aβ and α-syn (Table S2).

Seeding capacities of self-seeded T40 fibrils and AD-tau were compared with heparin-induced T40 (Hep-T40) fibrils in non-Tg hippocampal or cortical neurons. Consistent with our previous study (Guo and Lee, 2013), treatment with Hep-T40 fibrils resulted in limited aggregation of endogenous mouse tau, manifested as rare puncta labeled by a mouse tau–specific antibody in methanol-fixed neurons (Fig. 2, A and C). In contrast, cofactor-free self-seeding sometimes generated a unique variant of T40 fibrils (hereafter referred to as X-T40 fibrils) capable of inducing profuse thread-like mouse tau aggregates, which were also observed when non-Tg neurons were treated with AD-tau (Fig. 2, A and B). For both variants, the widespread mouse tau pathology mostly stayed in the axons, although occasional perikaryal depositions occurred with X-T40 treatment (Fig. 2 D).

To rule out the possibility that contaminants in AD-tau preparations nonspecifically caused abnormal tau accumulations, we performed immunodepletion of tau from these preparations and found abolishment of seeding activity in neurons (Fig. 2, E and F). Furthermore, when added together with synthetic tau fibrils to non-Tg neurons, AD-tau preparations that had been immunodepleted of tau neither enhanced the seeding activity of Hep-T40 fibrils (Fig. 2 G compared with Fig. 2 A) nor altered the pattern of tau pathology induced by X-T40 fibrils (Fig. 2 H compared with Fig. 2 A), suggesting extrinsic factors present in AD-tau preparations do not directly influence the seeding properties of tau fibrils. Collectively, these results support the idea that tau fibrils purified from AD brains are intrinsically different from synthetic tau fibrils.

Additionally, the differential activity of Hep-T40, X-T40, and AD-tau fibrils in inducing endogenous tau pathology was confirmed biochemically through immunoblotting of sarkosyl-soluble and -insoluble fractions from treated neurons (Fig. 2 K). Although cultured non-Tg neurons express both 3R and 4R mouse tau (Fig. 2, I and J), only 4R tau was recruited into the insoluble fraction by X-T40 fibrils, but both 3R and 4R tau were recruited by AD-tau (Fig. 2 K).

AD-tau induces and propagates abundant tau pathology in non-Tg mice

We further tested whether these tau fibril variants can propagate tau pathology in young (2–3 mo) non-Tg mice after a single unilateral injection into the dorsal hippocampus and overlying cortex (Fig. 3 A). Consistent with poor seeding in cultured neurons, inoculation of 9 μg Hep-T40 fibrils failed to induce appreciable tau pathology up to 24 mo postinjection (p.i.; Fig. 3, B and C). Despite considerable variability among injected animals, 9 μg X-T40 fibrils overall resulted in only a small number of tau inclusions, detected by phospho-tau antibody AT8 (pS202 and T205), in the ipsilateral hippocampus up to 9 mo p.i. (Fig. 3, B and D). In stark contrast, inoculation of 8 μg or even 2 μg AD-tau gave rise to numerous AT8-positive tau aggregates in several brain regions as early as 3 mo p.i. (Figs. 3 B and Fig. 4 A). This result was confirmed with inoculation of 2 μg AD-tau independently prepared from two additional AD cases (not depicted and Table S4).

To eliminate the possibility of detecting residual AD-tau, we monitored inoculated human tau using both AT8 and human tau–specific antibody HT7 at earlier time points and

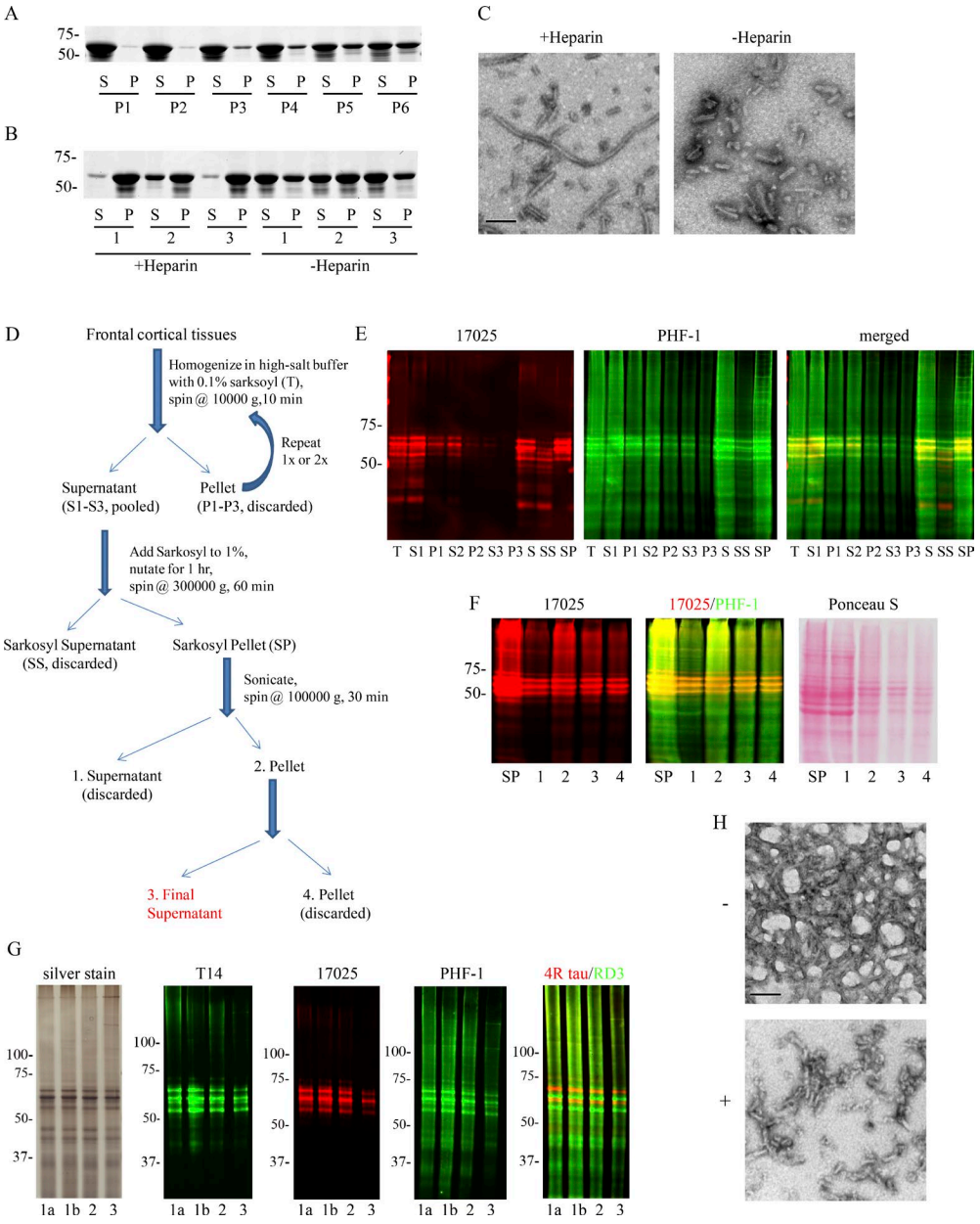

Figure 1. **Preparation of different variants of tau fibrils.** (A) Sedimentation test for passages 1–6 of repetitively self-seeded T40 fibrillization without heparin. Supernatant (S) and pellet (P) fractions were resolved on SDS-PAGE and stained by Coomassie blue. Data are representative of more than three independent fibrillization series. (B) Sedimentation test for T40 fibrils induced with and without heparin; three different preparations are shown for each category. The heparin-free fibrils were from passages 9 or 10 of repetitively self-seeded fibrillization as shown in A. (C) Negative staining EM images for T40 fibrils induced with and without heparin after sonication. Bar, 100 nm. (D) A schematic diagram summarizing the main steps of tau PHF purification from AD brains. (E and F) Different fractions from PHF purification (refer to the schematic in D) were immunoblotted with 17025 (a polyclonal pan-tau antibody) and PHF-1 (a monoclonal antibody specific for tau phosphorylated at S396/S404). (F) Ponceau S staining for the final purification steps revealed further removal of contaminants from the sarkosyl pellet. The final supernatant (fraction 3, red in D) is the fraction used in the study and referred to as AD-tau. Data are representative of at least eight independent extractions (Table S2). (G) Silver staining of AD-tau shows prominent bands between 50 and 75 kD, recognized by a panel of tau antibodies, including T14 (a monoclonal antibody specific for human tau), 17025, PHF-1, RD3 (a 3R tau-specific monoclonal antibody), and an anti-4R tau polyclonal antibody. Representative preparations from the frontal cortices of three AD cases are shown (1a and 1b are two different preparations from the same case). (H) Negative staining EM images for AD-tau with (+) and without (−) sonication. Bar, 100 nm. (A, B, and E–G) Molecular mass is indicated in kilodaltons.

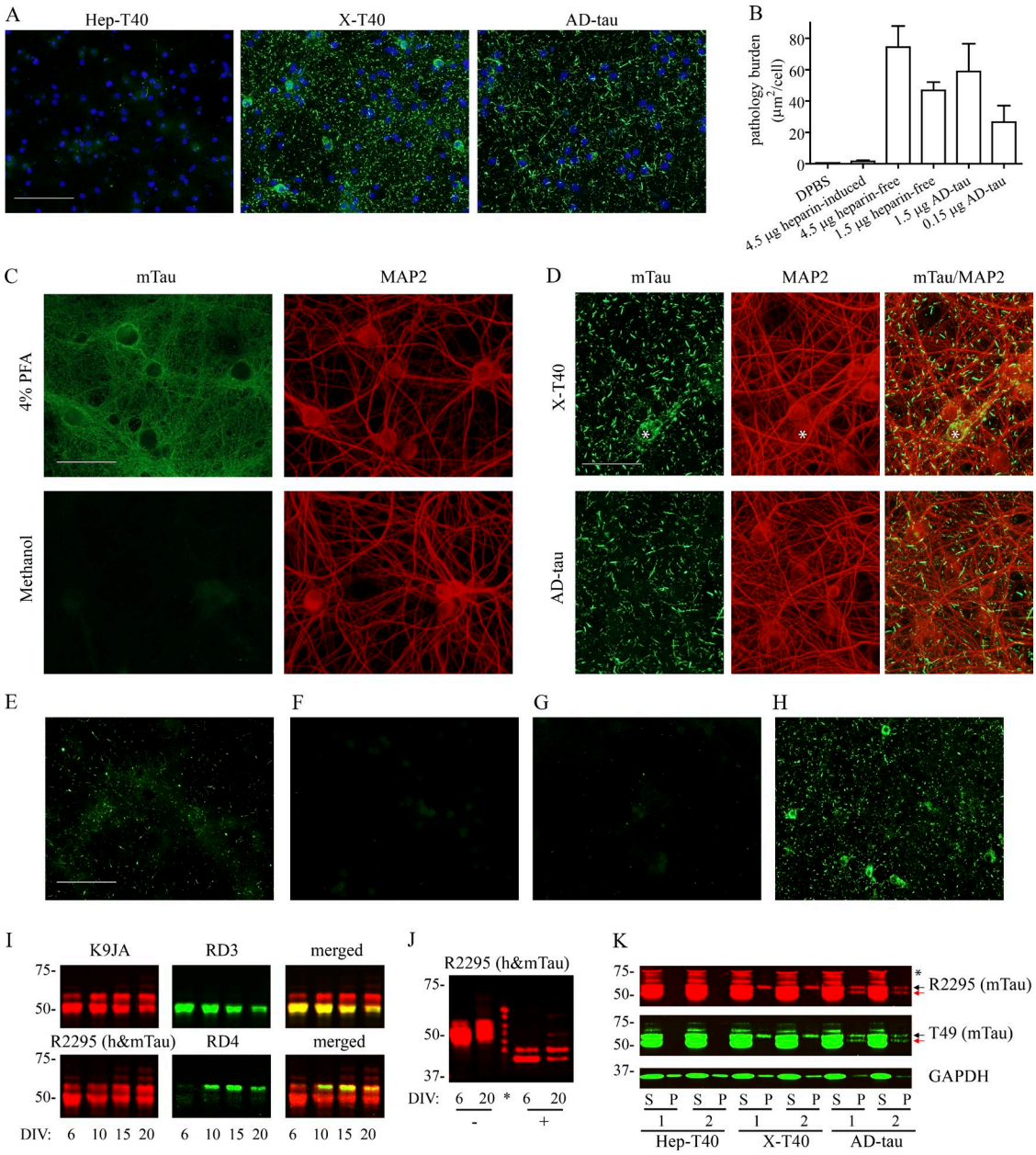

Figure 2. **Different variants of tau fibrils differentially seed tau pathology in non-Tg neurons.** (A) Induction of endogenous mouse tau pathology in non-Tg neurons treated with the different variants of tau fibrils (amount of tau per coverslip: 4.5 µg for Hep-T40 and X-T40; 1.5 µg for AD-tau). Neurons were fixed with methanol to remove soluble tau (Fig. 2 C) and immunostained with T49, a mouse tau–specific monoclonal antibody (green). Data are representative of more than three independent experiments. Bar, 100 µm. (B) Quantification of the area occupied by mouse tau pathology normalized to total cell count, shown as mean + SEM. For each fibril variant, three different preparations were tested across three independent sets of neurons; AD-tau preparations from three different cases were tested. (C) Immunostaining of mouse tau (mTau; T49; green) and MAP2 (polyclonal antibody 17028; red) in DPBS-treated non-Tg neurons fixed with 4% PFA or with cold methanol. In these control neurons, MAP2 immunoreactivity, which is in the neuronal cell bodies and dendrites, remains intact with methanol extraction, but the axonally located mouse tau is largely removed by methanol fixing. The results are verified in two independent experiments. Bar, 50 µm. (D) The thread-like neuritic tau aggregates induced by both X-T40 and AD-tau fibrils rarely colocalized with MAP2 staining, suggesting their axonal location. X-T40 but not AD-tau fibrils induced tau aggregation in a subset of neuronal cell bodies (shown by asterisks in the top panels). Bar, 50 µm. (E and F) Mouse tau pathology induced by AD-tau preparations after a mock immunodepletion using control mouse IgG (E) or after immunodepletion of tau using Tau 5 (F). The volume of unbound fraction added per coverslip contained 0.2 µg of AD-tau before immunodepletion. Seeding activity of AD-tau was abolished by Tau 5 but not by the control mouse IgG. (G and H) Mouse tau pathology induced by 4.5 µg Hep-T40 fibrils (G) or 1.5 µg X-T40 fibrils (H) that had been mixed with tau-immunodepleted AD-tau preparations. (E–H) Images are representative of three AD cases tested. Bar, 100 µm. (I) RIPA-extracted lysates from non-Tg neurons that were 6, 10, 15, and 20 d in vitro (DIV) were probed for 3R and 4R tau expression

found visible immunoreactivities around the injection sites at 2 d p.i. but not at 7 d p.i. (Fig. 5, A and B). Thus, AT8 immunoreactivities detected thereafter must represent endogenous mouse tau recruited by injected AD-tau that was internalized and survived degradation. This was confirmed by labeling of the tau inclusions by mouse tau–specific antibody R2295 (Fig. 5 E). Moreover, inoculation of control brain extracts containing equivalent concentrations of total proteins but little abnormal tau did not result in any tau pathology (Tables S1 and S2 and Fig. 5 F), thus excluding any nonspecific induction of tau aggregation by injection-associated brain damage or by exposure to human brain materials.

Unexpectedly, only modest neuropil accumulations of tau ever developed near the injection sites after the clearance of inoculated AD-tau (Fig. 5, C and D), whereas abundant perikaryal inclusions were observed in brain regions anatomically connected to the injection sites, such as the polymorphic layer (hilus) of the ventral dentate gyrus on both ipsilateral and contralateral sides, the raphe nucleus, and the mammillary area (Fig. 3 B and Fig. 4 A). Tau pathology in the abovementioned regions persisted up to 9 mo p.i., with 8-μg but not 2-μg injections leading to significantly more pathology at 9 mo p.i. than at 3 mo p.i. in the ipsilateral ventral hippocampal hilus (Fig. 3 F and Fig. 4 B). Meanwhile, new inclusions emerged starting 6 mo p.i. in a few distal sites, including the locus coeruleus (Fig. 3 E, Fig. 4 A, and Fig. 6 A). Together, these results provide evidence for retrograde (and possibly anterograde) transmission of pathological tau and selective vulnerability of different neuronal populations to the development of tau pathology in non-Tg mice (Fig. 6 B). Furthermore, other markers of tau pathology (AT180, TG3, and MC1) displayed increased immunoreactivities over time, with a subset of tau inclusions turning ThS positive, indicating time-dependent maturation of pretangles into NFT-like aggregates (Fig. 6, C and D). However, no overt neuron loss was ever detected up to 9 mo p.i., even in the ventral hippocampal hilus where the highest density of tau pathology developed (Fig. 3 G and Fig 4 C).

We also performed AD-tau inoculation into aged (15–19 mo) non-Tg mice, in which a very similar pattern of induction and propagation of tau pathology was observed. Interestingly, although inoculation of 2 μg AD-tau led to minimal pathology in the ipsilateral entorhinal cortex of young non-Tg mice, the same low dose of AD-tau resulted in appreciable pathology in the ipsilateral entorhinal cortex of mice injected at 15–19 mo old (Fig. 4, D and E). In addition, more pronounced neuropil accumulations of tau were observed in the aged mice at 6 mo p.i. in several white matter regions, such as the fimbria and corpus callosum (Fig. 4, D, F, and G). Therefore, the age of mice appears to have a modifying effect on the spreading of AD-tau–induced tau pathology.

Elucidating structural arrangement of 4R and 3R tau in AD PHFs

Next, we tried to identify unique structural features of AD-tau that could underlie its higher seeding activity. AD PHFs are known to consist of both 4R and 3R tau at an ∼1:1 ratio (Lee et al., 2001), but the exact structural relationship between 4R and 3R tau within filaments is unclear because epitopes that distinguish these isoforms are in the MT-binding repeat domains, which are deeply buried in the fibril core (Goedert et al., 1996; von Bergen et al., 2006; Espinoza et al., 2008). Three models of 4R/3R tau arrangement in PHFs are conceivable (Fig. 7 A): (1) alternating 4R and 3R tau molecules are obligatory building blocks, (2) 4R and 3R tau segregate into distinct fibrils that do not cross-seed, and (3) 4R and 3R tau can coassemble into the same fibrils in a random, nonobligatory manner. To identify the correct model and also circumvent difficulties in analyzing AD PHFs directly, we adopted an alternative strategy of examining rTau fibrils templated by AD PHFs, whereby 10% AD-tau seeds were incubated with human rTau T40 (4R2N) and T39 (3R2N) monomers, either separately or mixed at a 1:1 ratio at the same total protein concentration. In a subset of experiments, we attached a Myc tag to T40 and a hemagglutinin (HA) tag to T39 at the C terminus, which would be positioned outside the fibril core and thereby allow visualization of incorporated rTau.

In the presence of 10% AD-tau seeds, ∼30% of starting rTau monomers (with or without tags) were incorporated into the insoluble fraction regardless of single- or mixed-isoform fibrillization (Fig. 7, C–E), whereas rTau alone remained largely soluble under the same fibrillization condition (Fig. 7 B). This is different from heparin-induced fibrillization, wherein 3R tau was reported to inhibit fibrillization of 4R tau (Adams et al., 2010). Immuno-EM of singly seeded Myc-T40 and HA-T39 (designated as [AD]Myc-T40 and [AD] HA-T39) showed abundant filaments labeled by anti-Myc or anti-HA antibodies proximal to stretches of PHF-1 (pS396/

using isoform-specific monoclonal antibodies RD3 and RD4, respectively. Total tau was shown by K9JA (a polyclonal antibody recognizing residues 243–441 of tau) or R2295 h&mTau (a fraction of polyclonal serum recognizing both human and mouse tau). Data are representative of three independent sets of neurons tested. (J) Dephosphorylation of neuronal lysates showed that the two predominant isoforms of mouse tau expressed in culture are the shortest ones (i.e., 3R0N and 4R0N) when aligned to the six isoforms of human tau (the lane marked by an asterisk). The blot was probed with R2295 h&mTau. Because a mouse tau sequence is shorter than a human tau, 4R0N mouse tau is aligned with 3R0N human tau, and 3R0N mouse tau runs even lower. Three dephosphorylation experiments were performed on two independent sets of neuronal lysates. (K) Supernatant (S) and pellet (P) fractions from 1% sarkosyl extraction of treated non-Tg neurons were immunoblotted with mouse tau (mTau)–specific antibodies (R2295 and T49), with two preparations of fibrils tested for each variant (9 μg Hep-T40, 3 μg X-T40, and 3 μg AD-tau for each well on a 12-well plate). Black and red arrows indicate 4R and 3R mouse tau, respectively. The asterisk indicates a nonspecific band detected by R2295. Data are representative of three independent sets of non-Tg neurons tested. (I–K) Molecular mass is indicated in kilodaltons.

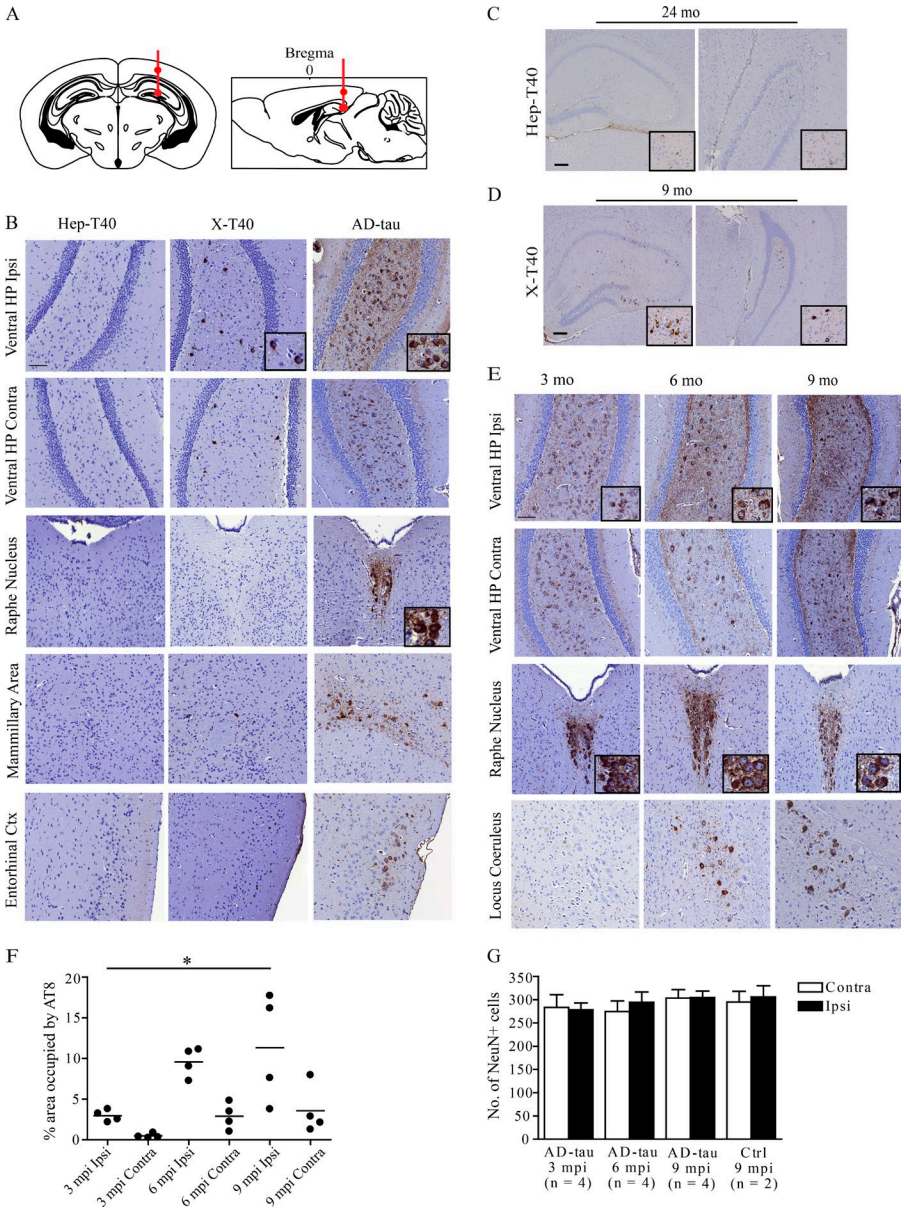

Figure 3. **AD-tau is a more potent seed for tau aggregation in non-Tg mice.** (A) Schematics showing injection sites in the dorsal hippocampus and overlying cortex indicated by red dots (Bregma −2.54 mm, 2 mm from midline, and −1.4 mm from skull [for the cortex] and −2.4 mm from skull [for the hippocampus]). (B) Differential induction of tau pathology recognized by AT8 (a monoclonal antibody specific for tau phosphorylated at S202/T205) in non-Tg mice at 3 mo p.i. of different tau fibrils. Amount of tau injected per mouse: 9 µg for Hep-T40 (four mice) and X-T40 fibrils (six mice); 8 µg for AD-tau (four mice). Contra, contralateral; Ctx, cortex; HP, hippocampus; Ipsi, ipsilateral. Bar, 100 µm. (C) AT8 immunostaining at 24 mo p.i. of Hep-T40 fibrils (9 µg/mouse; two mice). (D) AT8 immunostaining at 9 mo p.i. of X-T40 fibrils (9 µg/mouse; three mice). Considerable variability was found among injected animals, with the one mouse developing the most abundant pathology shown here. (C and D) Bars, 200 µm. (E) AT8 immunostaining at 3, 6, and 9 mo p.i. of AD-tau (8 µg/mouse; four mice per time point). Bar, 100 µm. (F) Quantification of percent area occupied by AT8-positive tau pathology developed in the ventral hippocampal hilus with 8 µg AD-tau injection (four mice per time point; each dot represents one mouse). One-way ANOVA was performed across different time points for ipsilateral and contralateral pathology separately. Significant differences were found for ipsilateral pathology, and Tukey's multiple comparison test identified a significant difference between 3 and 9 mo p.i. *, $P < 0.05$. mpi, months p.i. (G) AD-tau inoculation (8 µg/mouse) did not lead to significant neuron loss in the ventral hippocampal hilus region as compared with mice injected with control (Ctrl) brain extracts. Data are shown as mean + SEM. One-way ANOVA found no significant differences among the groups. Data shown in this figure were obtained from injections performed all on 2–3-mo-old non-Tg mice (C57BL6 or C57BL6/C3H F1). Refer to Table S4 for the details of animals analyzed per group.

S404 tau)–positive AD-tau (Fig. 7 F), indicating successful templated recruitment of rTau by AD PHFs, as previously shown for 4R0N rTau (Morozova et al., 2013). The observation that 4R or 3R rTau alone can be recruited by AD PHFs to form fibrils suggests the unlikelihood of model 1, which was also argued against by the induction of tau pathology by AD-tau inoculation in adult mouse brains, which only express 4R tau (Fig. 3). Furthermore, immuno-EM on co-seeded Myc-T40 and HA-T39 (i.e., [AD]Myc-T40 + HA-T39) revealed frequent occurrences of individual filaments decorated by both anti-Myc and anti-HA antibodies amid occasional filaments with single immunoreactivity (Fig. 7, G–I), suggesting model 3 is the most accurate model (Fig. 7 A).

Propagation of AD-tau seeding properties to rTau

To determine whether rTau fibrils seeded by AD-tau inherit biological properties of their parental seeds, we tested their activities in cultured non-Tg neurons. Indeed, [AD]T40, [AD]T39, and [AD]T40 + T39 all elicited significantly more abundant tau pathology than the 10% AD-tau seed control, and the exclusive neuritic localization of induced tau aggregates phenocopies their parental seeds (Fig. 8, A and B). Immu-

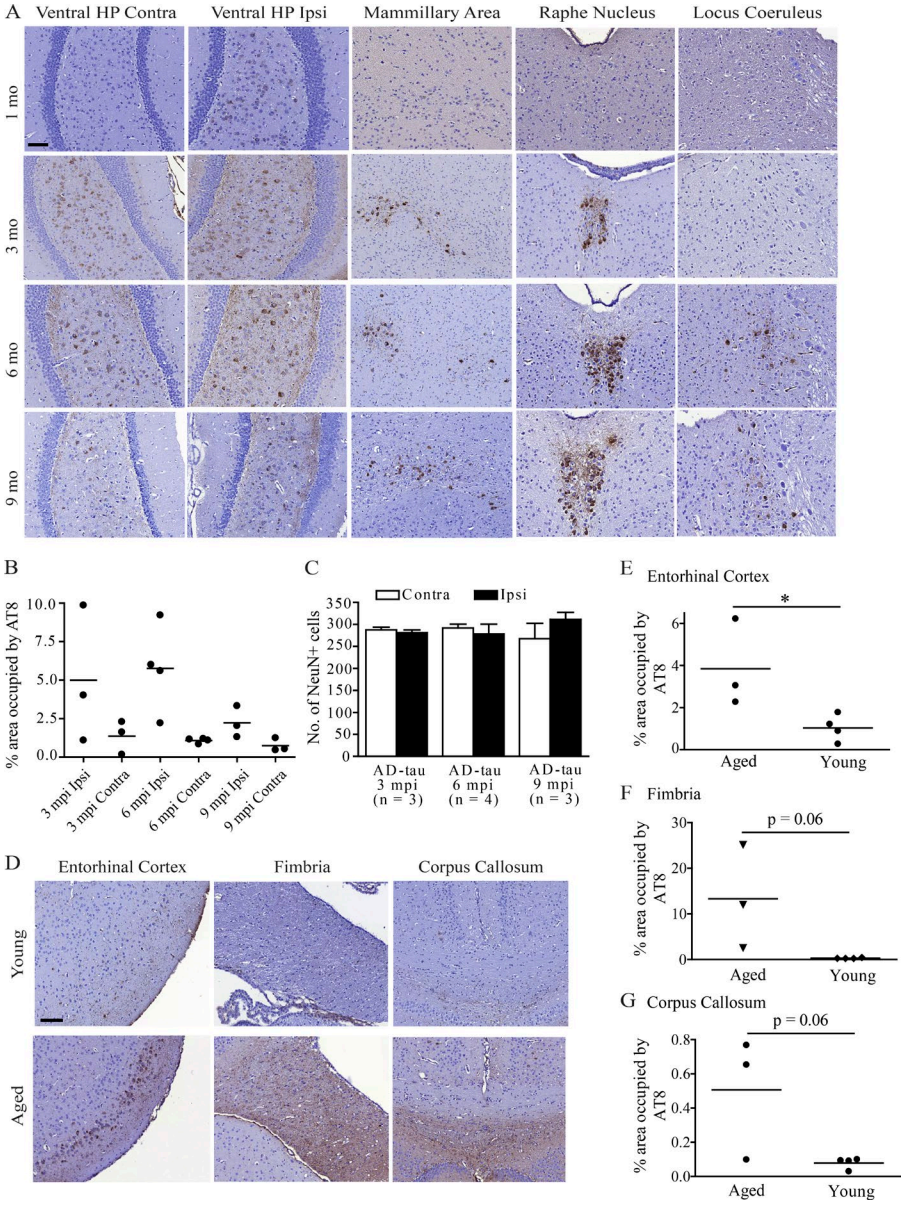

Figure 4. **Propagation of tau pathology after inoculation of a lower dose of AD-tau into young and aged non-Tg mice.** (A) AT8 immunostaining for various brain regions after a lower dose of AD-tau inoculation (2 µg/mouse) into the dorsal hippocampus (HP) and overlying cortex of 2–3-mo-old non-Tg mice (C57BL6). Only weak AT8 immunoreactivities were detected in the ipsilateral (Ipsi) ventral hippocampus at 1 mo p.i. (three mice). More prominent AT8-positive tau inclusions appeared in both the ipsilateral and contralateral (Contra) ventral hippocampus at 3 mo p.i. (three mice), which showed a trend of decline between 6 and 9 mo p.i. (four and three mice, respectively). Bar, 100 µm. (B) Quantification of percent area occupied by AT8-positive tau pathology developed in the ventral hippocampal hilus with 2-µg AD-tau injection (three to four mice per time point; each dot represents one mouse). (C) Quantification of NeuN$^+$ cells in the ventral hippocampal hilus region with 2-µg AD-tau injection. Data are shown as mean + SEM. (B and C) One-way ANOVA showed no significant differences among groups. (D) Comparisons of AT8-positive tau pathology developed in the ipsilateral entorhinal cortex, ipsilateral fimbria, and corpus callosum at 6 mo p.i. of AD-tau into young (2–3 mo) versus aged (15–19 mo) non-Tg mice (2 µg/mouse; four young and three aged mice at 6 mo p.i. with each dot representing one mouse; all C57BL6). Bar, 100 µm. (E–G) Quantification of percent area occupied by AT8 immunoreactivities in regions shown in D followed by Student's *t* tests indicated that aged mice developed significantly more pathology in the ipsilateral entorhinal cortex (*, $P < 0.05$) and a trend of more abundant pathology in the ipsilateral fimbria and corpus callosum. Data represent three to four mice per time point; each dot represents one mouse.

noblotting of neuronal lysates confirmed endogenous mouse tau was recruited into the sarkosyl-insoluble fraction beyond what could be attributed to the 10% seeds (Fig. 8 C). These results suggest successful amplification of seeding-competent AD-tau conformers with rTau. Importantly, insoluble mouse tau recovered from neurons invariably consisted of an equal ratio of 4R and 3R mouse tau, regardless of whether the exogenous fibrils were composed of mostly 4R or 3R human rTau (Fig. 8 C). This observation lends further support for model 3 because model 2 would entail differential recruitment of 4R and 3R mouse tau by [AD]T40 and [AD]T39, respectively (Fig. 7 A). Unlike the structural equivalency of 4R and 3R tau in AD PHF assembly, 3R tau isoforms are significantly impaired in acquiring the neuronal seeding properties of X-T40 fibrils as compared with 4R tau isoforms (Fig. 7, D and E), suggesting a conformational barrier between the isoforms for this particular variant of fibrils, similar to what has been demonstrated in cell-free systems for heparin-induced tau fibrils (Dinkel et al., 2011; Siddiqua et al., 2012).

We noted that rTau fibrils seeded by AD-tau were less potent than an equal mass of AD-tau in seeding endogenous mouse tau pathology in non-Tg neurons (Fig. 8 B), but this could be explained by only ∼30% of rTau turning insoluble upon seeding (Fig. 7 E), as only the pelletable fraction exhibited appreciable seeding activity (not depicted). Although rTau remaining in the soluble fraction appeared to be C-terminally truncated by unknown proteases copurified with AD-tau (Fig. 7, C and D), an additional boiling step included during purification eliminated the protease activity without augmenting the amount of pelletable tau (not depicted), im-

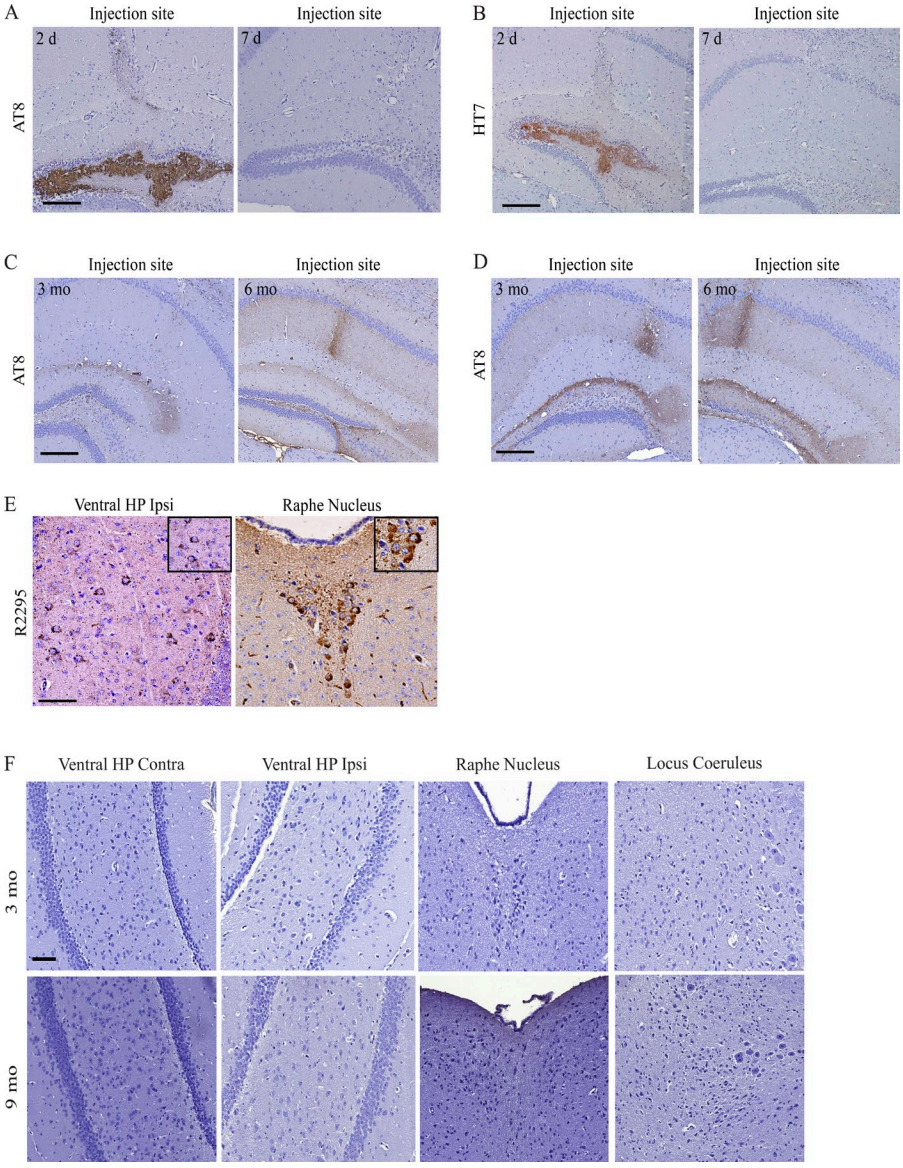

Figure 5. **Pathology developed after AD-tau inoculation is composed of endogenous mouse tau and cannot be induced by control brain extracts.** (A and B) IHC of the injection site with AT8- and human tau–specific antibody HT7 at 2 and 7 d p.i. (2 µg/mouse; two mice per time point). (C and D) AT8-positive neuropil staining, presumably caused by endogenous mouse tau accumulations, was observed near the injection site at 3 and 6 mo p.i. (2 µg/mouse for C; 8 µg/mouse for D; four mice per condition except for three mice at 3 mo p.i. of 2 µg/mouse). (E) IHC with mouse tau–specific R2295 confirms recruitment of endogenous mouse tau into aggregates formed in the ipsilateral ventral hippocampus (Ventral HP Ipsi) and raphe nucleus at 3 mo p.i. (8 µg/mouse; four mice). (F) Lack of AT8 immunoreactivity throughout the brains after injections of extracts from control brains prepared the same way as AD-tau. Bars: (A–D) 200 µm; (E and F) 100 µm. Data shown in this figure were obtained from injections performed all on 2–3-mo-old C57BL6 mice.

plying that other variables rather than the availability of soluble tau are limiting templated recruitment.

Because AD PHFs consist of all six isoforms of tau that are hyperphosphorylated, we performed an in vitro kinase assay to generate phosphorylated recombinant T40 (Fig. 9 A) and then tested the ability of phosphorylated T40 as well as a mixture of all six isoforms of rTau to propagate AD-tau conformation in vitro. However, neither substrate showed enhanced recruitment into the insoluble fraction by AD-tau compared with untreated T40 or T39 (Fig. 9, B and C, compared with Fig. 7 C). Consequently, neither substrate seeded by AD-tau induced more abundant pathology in non-Tg neurons than equivalently seeded nonphosphorylated T40 (Fig. 9, D–G). Therefore, the phosphorylation status of tau and the exact complement of tau isoforms do not appear to significantly influence in vitro propagation of AD-tau. We speculate that in vitro reactions may be lacking certain intracellular factors required for efficient amplification of AD-tau conformers.

Molecular basis of differential seeding activities

To verify that the distinct variants of tau fibrils with differential seeding activities are structurally different, Hep-T40, X-T40, and [AD]T40 fibrils were treated with increasing concentrations of trypsin, and indeed three distinct patterns of trypsin-resistant fragments were observed (Fig. 10 A). A direct comparison was not made with AD-tau because of complexity arising from tau hyperphosphorylation and the presence of all six isoforms, but [AD]T40 fibrils presumably have adopted at least some conformational aspects of AD-tau based on amplified seeding activity in neurons (Fig. 8, A–C). Digestion by higher concentrations of trypsin revealed clear, albeit distinct, resistant domains for Hep-T40 and [AD]T40

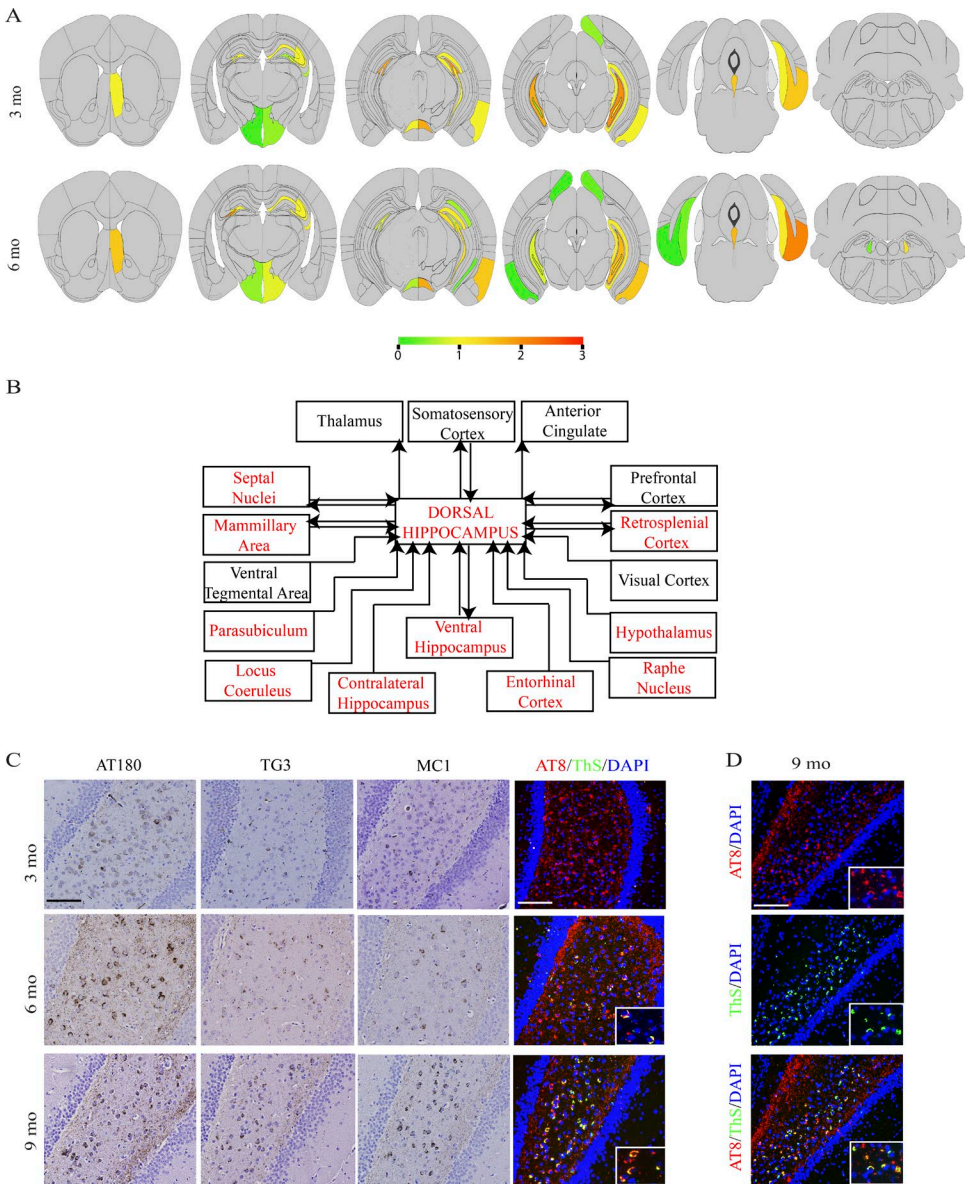

Figure 6. **Spreading and maturation of tau pathology induced by AD-tau inoculation in non-Tg mice.** (A) Heat maps showing semiquantitative analyses of tau pathology based on AT8 immunostaining (0: no pathology, gray; 3: maximum pathology, red) at 3 and 6 mo p.i. of AD-tau (8 µg/mouse; four mice per time point). Six coronal planes are shown from left to right: bregma 0.98 mm, −2.18 mm, −2.92 mm, −3.52 mm, −4.96, and −5.52 mm. The distribution of tau pathology at 9 mo p.i. is very similar to that at 6 mo p.i. (not depicted). (B) A schematic showing various brain regions connected to the dorsal hippocampus, the primary site receiving inoculums (Fig. 5, A and B), with both afferents and efferents indicated by directional arrows. Brain regions with tau aggregate formation after AD-tau injections are marked in red. The diagram was created based on data from the Allen Brain Atlas C57BL/6 mouse connectivity studies (Oh et al., 2014). (C) Brain sections were immunostained with antibodies AT180 (recognizing tau phosphorylated at T231), MC1 (recognizing a pathological conformation of tau found in the AD brains), and TG3 (recognizing conformationally altered tau phosphorylated at T231), which all demonstrated increased immunoreactivities over time after AD-tau inoculation (8 µg/mouse; four mice per time point). Double-labeling immunofluorescence using AT8 (red) and ThS (green) shows a subset of pretangles matured into β sheet–rich tangle-like aggregates starting 6 mo p.i. (D) AT8 and ThS double labeling of the ipsilateral ventral hippocampus at 9 mo p.i. of AD-tau (8 µg/mouse; four mice). Bars, 100 µm. Data shown in this figure were obtained from injections performed all on 2–3-mo-old C57BL6 mice.

fibrils that were ∼12 and ∼18 kD in size, respectively, but there is less of a well-defined resistant fragment for X-T40 fibrils. Immunoblotting of trypsin-resistant tau fragments using antibodies recognizing different domains of tau showed that, as expected, the MT-binding repeat region is the most shielded domain, whereas the N terminus is the most accessible to trypsin digestion for all variants (Fig. 10 B). Among the three fibril variants, both the N and C termini of tau ap-

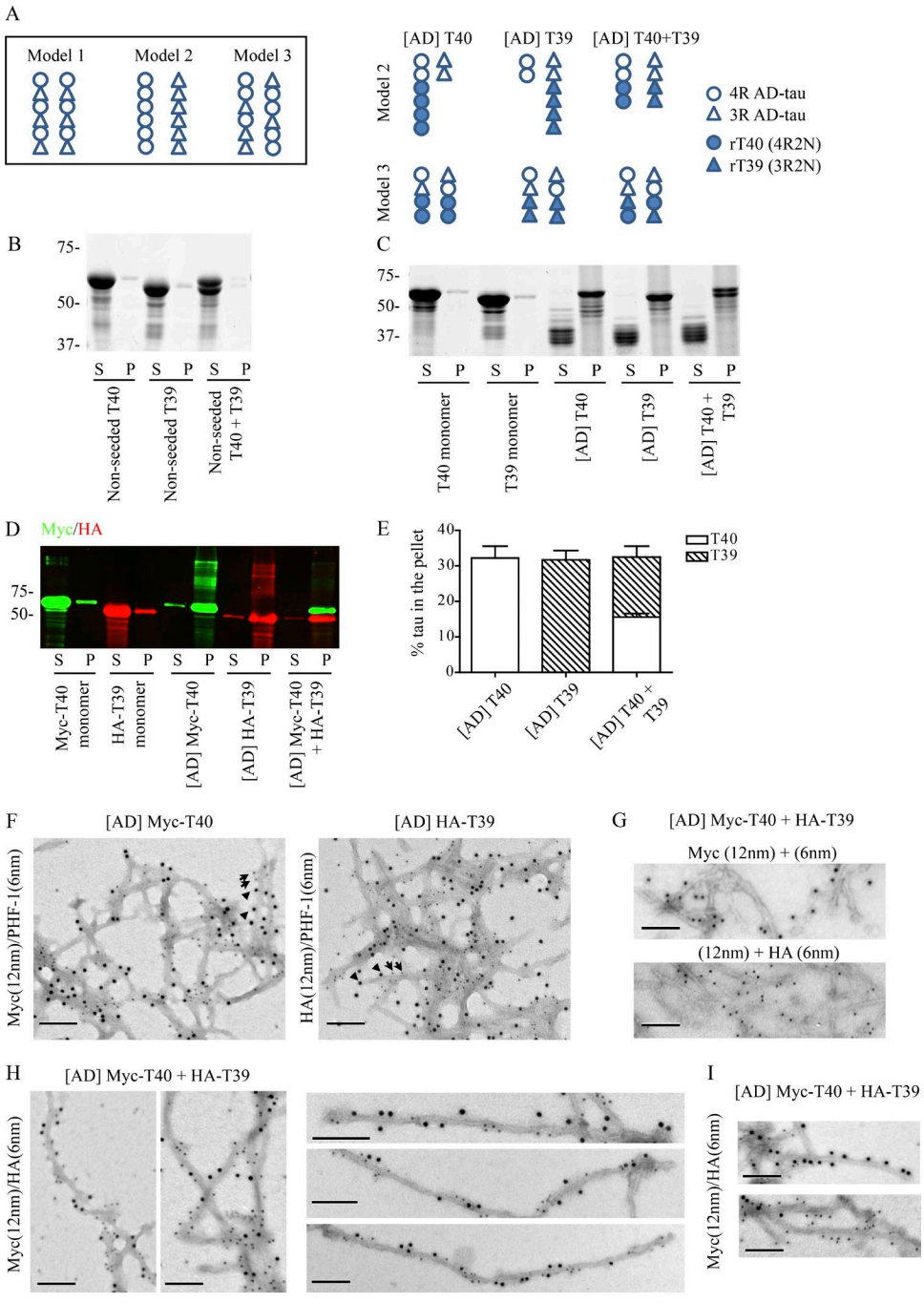

Figure 7. **rTau fibrils templated by AD-tau reveal structural relationship between 4R and 3R tau.** (A) Three possible models of 4R/3R tau arrangement in AD PHFs (left) and proposed patterns of recombinant T40/T39 (rT40/rT39) recruitment by AD-tau based on models 2 and 3 (right). (B) Sedimentation test for nonseeded T40 and T39 after 3-d incubation at 37°C with constant agitation at 1,000 rpm. Cofibrillization was conducted at the same total protein concentration as single-isoform fibrillization with T40 and T39 mixed at a 1:1 ratio. S, supernatant; P, pellet. (C) Sedimentation test for singly or cofibrillized T40 and T39 seeded by 10% AD-tau ([AD]T40, [AD]T39, and [AD]T40 + T39) under the same fibrillization condition as in B. Monomers were used as the controls. rTau remaining in the soluble fraction appeared to be truncated. (D) Sedimentation test for singly or cofibrillized Myc-T40 and HA-T39 seeded by 10% AD-tau ([AD]Myc-T40, [AD]HA-T39, and [AD]Myc-T40 + HA-T39) under the same fibrillization condition as in B, with monomers as the controls. Supernatant and pellet fractions were immunoblotted with anti-Myc and anti-HA antibodies. These two antibodies do not label truncated tau in the supernatant as seen in C, suggesting the C terminus of tau was cleaved together with the tag. (B–D) Data shown are representative of at least two independent experiments. (E) Quantification for the percentage of starting tau monomers recruited into the pellet fraction with AD-tau seeding as shown in C and D. Data are displayed as mean + SEM and are based on three independent experiments. (F) Double-labeling immuno-EM images for [AD]Myc-T40 and [AD]HA-T39 fibrils, stained with PHF-1 and anti-Myc or anti-HA antibody. Secondary antibodies are conjugated to colloidal gold particles of two different sizes (6 nm or 12 nm).

pear to be the most exposed in [AD]T40 fibrils, whereas the C terminus seems to be the most preserved in X-T40 fibrils. Structural differences among the three variants were further confirmed by proteinase K digestion, which also presented three distinct banding patterns (Fig. 10 C).

Besides conformational differences, the poor seeding by Hep-T40 fibrils could be partly caused by the inhibitory effect of heparin on fibril internalization, as heparin competes with cell-surface heparan sulfate for binding to tau fibrils (Holmes et al., 2013). Although Hep-T40 fibrils were pelleted and resuspended in heparin-free buffer before being added to neurons, heparin has been reported to form a tight complex with tau during fibrillization (Zhu et al., 2010), and a dose of heparin equivalent to that contained in our Hep-T40 fibrils was found to significantly reduce the seeding efficacy of X-T40 and AD-tau fibrils in cultured neurons (Fig. 10, D and E).

DISCUSSION

In recent years, a rapidly growing body of literature has reinforced the hypothesis that prion-like, cell-to-cell transmission of amyloid protein aggregates underlies disease progression of numerous neurodegenerative disorders (Guo and Lee, 2014; Walker and Jucker, 2015). Unsatisfactorily, except for PrP^{Sc} (Weissmann et al., 2002) and α-syn (Luk et al., 2012a; Masuda-Suzukake et al., 2013; Paumier et al., 2015), templated induction and propagation of other disease-associated protein aggregates have never been robustly demonstrated in non-Tg animals without overexpression of the respective proteins (Guo and Lee, 2014). This shortcoming has left lingering doubts on whether experimental evidence supporting the transmission hypothesis, predominantly from Tg animals, is applicable to neurodegenerative diseases in humans where the disease-associated proteins are almost never up-regulated.

We hypothesized that difficulties in generating significant tau pathology in non-Tg animals were partly caused by the use of suboptimal seeding materials. Studies from us and others showed that amyloid aggregates composed of one single protein can exhibit different conformations (Petkova et al., 2005; Furukawa et al., 2011; Guo et al., 2013; Sanders et al., 2014; Peelaerts et al., 2015), and we previously described distinct conformational variants of synthetic α-syn fibrils with differential seeding capacity (Guo et al., 2013). Although artificially generated tau fibrils induced by heparin have been used extensively to propagate tau pathology in Tg mice overexpressing mutant tau (Iba et al., 2013, 2015; Peeraer et al., 2015; Stancu et al., 2015), they are inefficient in templating fibrillization of non-overexpressed WT tau (Guo and Lee, 2013). Here, we demonstrate that authentic tau fibrils purified from AD brains (i.e., AD-tau) far surpass synthetic tau fibrils generated with or without heparin in seeding physiological levels of WT tau to aggregate in vivo. For the first time in non-Tg mice, abundant tau inclusions are convincingly induced in multiple brain regions that are anatomically connected within a few months after intracerebral inoculation of AD-tau. This observation provides the strongest support thus far for the pathophysiological relevance of tau transmission to human tauopathies, which are mostly sporadic. Importantly, we never detected injected materials (recognized by AT8 or HT7) in periventricular areas at 2 d or 7 d p.i., and the endogenous mouse tau pathology induced by AD-tau inoculation was also never observed in any periventricular areas up to 9 mo p.i. Therefore, the spreading of tau pathology observed in the inoculated non-Tg mice was unlikely caused by a simple leakage of AD-tau seeds into the ventricles. Although a previous study also tested inoculation of AD brain extracts into non-Tg mice, the extent of tau pathology induced in the brains of those injected mice was much lower than what we described here even after prolonged incubation, perhaps because of the use of crude brain homogenates which were not enriched with AD-tau in that study (Clavaguera et al., 2013).

Parallel with our findings of higher specific seeding activity of human brain–derived tau fibrils than synthetic tau fibrils, tau aggregates formed in tau Tg mice were shown to seed more efficiently than heparin-induced tau fibrils in cultured cells overexpressing mutant tau (Falcon et al., 2015). A similar discrepancy between synthetic- and brain-derived protein aggregates has been observed for other disease-associated proteins, including prion, Aβ, and α-syn (Colby and Prusiner, 2011; Luk et al., 2012b; Stöhr et al., 2012). We speculate that this phenomenon could be explained by three possible mechanisms. First, in vitro reactions cannot recreate the cellular milieu required for generating potent seeding conformers, including a lack of certain cofactors. Our study shows that even direct seeding by AD-tau cannot efficiently impart AD-tau conformation to rTau in vitro. Although heparin is a potent inducer of tau fibrillization in vitro, it is unlikely the intrinsic cofactor that initiates NFT formation, considering the low transmissibility of heparin-induced tau fibrils and their conformational difference from AD-tau. Heparin was also shown to interfere with propagation of the AD-tau conformation to rTau (Morozova et al., 2013). Second, posttranslational modifications of tau that are found in vivo are absent in rTau. Although phosphorylation of tau does not appear to promote

Arrowheads point to examples of Myc or HA immunoreactivity (12 nm), and arrows point to examples of PHF-1 immunoreactivity (6 nm). (G) Immuno-EM images of [AD]Myc-T40 + HA-T39 fibrils stained with a single primary antibody (anti-Myc alone at the top and anti-HA alone at the bottom) but with both secondary antibodies showed labeling by single-size gold particles, suggesting lack of nonspecific binding by secondary antibodies. (H and I) Double-labeling immuno-EM images for [AD]Myc-T40 + HA-T39 fibrils stained with both anti-Myc and anti-HA antibodies showed frequent intermingling of Myc (12 nm) and HA (6 nm) immunoreactivities on the same filaments (H) and occasional filaments with only Myc or only HA immunoreactivities (I). Bars, 100 nm. (F–I) Images are representative of at least two independent experiments. (B–D) Molecular mass is indicated in kilodaltons.

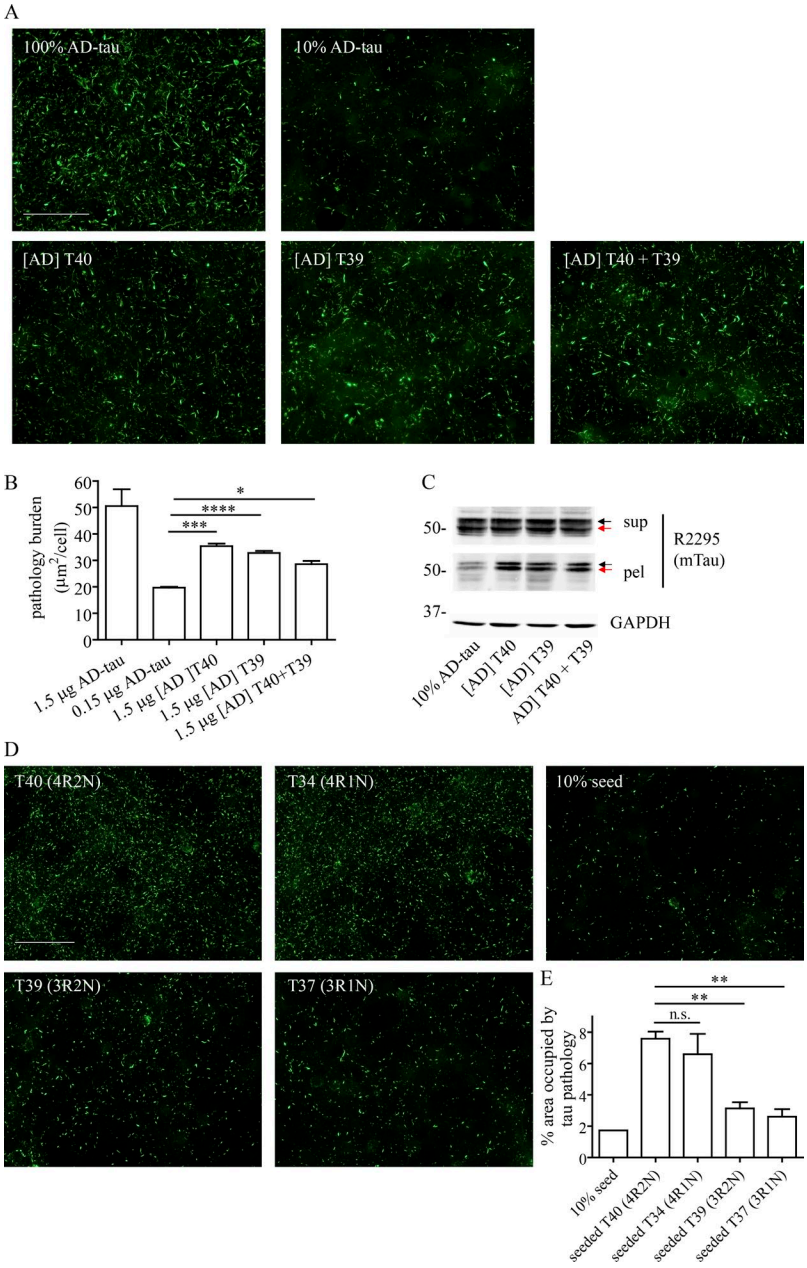

Figure 8. **rTau fibrils templated by AD-tau acquire seeding competency in non-Tg neurons.** (A) Mouse tau aggregates (methanol-resistant T49 staining in green) induced in non-Tg neurons by [AD]rTau fibrils compared with the same dose of AD-tau (100% AD-tau) and 10% AD-tau seed control (amount of tau per coverslip: 0.15 µg for 10% AD-tau and 1.5 µg for the rest). (B) Quantification of the area occupied by mouse tau pathology normalized to total cell count for the experiment shown in A, displayed as mean + SEM. Four different sets of [AD]rTau fibrils that were seeded by three different preparations of AD-tau were tested; two independent sets of non-Tg neurons were used. Pairwise Student's *t* tests were performed between seeded rTau fibrils and 10% seed control. *, $P < 0.05$; ***, $P < 0.0005$; ****, $P < 0.00005$. (C) Immunoblotting for sarkosyl-soluble (sup) and -insoluble (pel) fractions of non-Tg neurons treated with [AD]rTau fibrils or 10% AD-tau seed control (9 µg [AD]rTau and 0.9 µg AD-tau for each well on a 12-well plate). Black and red arrows indicate 4R and 3R mouse tau, respectively. Data are representative of two independent experiments. mTau, mouse Tau. Molecular mass is indicated in kilodaltons. (D) AT8-positive mouse tau pathology induced by different isoforms of tau seeded by 10% X-T40 fibrils. (E) Quantification of tau pathology for the experiment shown in D. The same preparation of X-T40 fibrils was used to seed different batches of independently purified monomers: four batches of monomers for T40 and two batches of monomers for T34, T39, and T37. Data are shown as mean + SEM. Pairwise Student's *t* tests were conducted between seeded T40 and the other isoforms. **, $P < 0.005$. Bars, 100 µm.

its seeding efficiency, as shown in this and another study (Falcon et al., 2015), we have not ruled out the effect of other modifications, including acetylation, glycosylation, ubiquitination, glycation, prolyl-isomerization, polyamination, oxidation, nitration, and sumoylation (Martin et al., 2011). Third, many different conformations of protein aggregates may arise in human brains, but the particular variants that dominate diseased brains are likely those that are kinetically favored, more resistant to degradation, and/or more readily transmitted than other misfolded conformers. In this regard, the emergence of such pathogenic tau conformers would be less likely to occur during in vitro fibrillization because processes that favor the selection of these pathogenic conformers over protracted periods of time in the brain are mostly missing in vitro. Hence, the unexpectedly low seeding activity of X-T40 fibrils in vivo could be caused by the lack of certain properties that are important for in vivo pathogenicity.

Our study also provides novel insights into the architectural arrangement of 4R and 3R tau in AD PHFs. Unlike most of the other tauopathies where tau aggregates are predominantly composed of either 4R (e.g., in corticobasal degeneration [CBD] and progressive supranuclear palsy [PSP]) or 3R tau (e.g., in Pick's disease), AD NFTs consist of an equimolar of 4R and 3R tau (Lee et al., 2001). Both in vitro and cell culture studies performed using heparin-induced tau fibrils showed very poor cross-seeding of 3R tau monomers

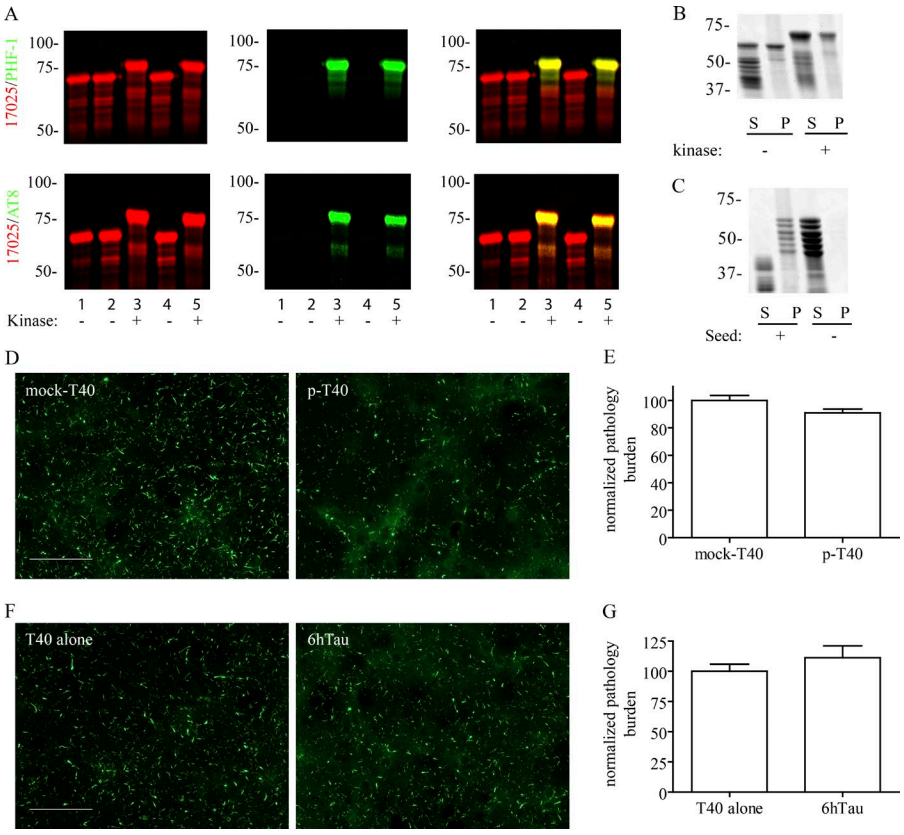

Figure 9. **Amplification of AD-tau using phosphorylated T40 and all six isoforms of tau.** (A) In vitro phosphorylation of T40 mediated by SAPK4. Lane 1: nontreated T40; lanes 2 and 4: mock-treated T40 in the same buffer condition as the phosphorylation reaction; lanes 3 and 5: T40 phosphorylated by incubation with SAPK4. Concentrations of T40 in the reactions were 12 µM for lanes 2 and 3 and 45 µM for lanes 4 and 5. The differently treated T40 was immunoblotted with 17025 and PHF-1 or AT8. (B) Sedimentation test for mock-treated T40 (–) and phosphorylated T40 (+) seeded by 10% AD-tau. (C) Sedimentation test for mixed six isoforms of tau with (+) and without (–) seeding by 10% AD-tau. (B and C) Reactions were incubated at 37°C for 3 d with constant agitation at 1,000 rpm. P, pellet; S, supernatant. Samples were resolved on SDS-PAGE and stained with Coomassie blue. (A–C) Data are representative of two independent experiments. Molecular mass is indicated in kilodaltons. (D and F) Methanol-resistant mouse tau pathology (T49 staining in green) induced by mock-treated T40 (mock-T40), phosphorylated T40 (p-T40), nontreated T40 (T40 alone), and six isoforms of tau (6hTau), all seeded by 10% AD-tau (1.5 µg tau added per coverslip). Bars, 100 µm. (E and G) Quantification of mouse tau pathology for experiments shown in D and F. Pathology was normalized to that induced by seeded mock-T40 (E) or seeded T40 alone (G) in each set of experiments. Data from two independent experiments are shown as mean + SEM. Student's *t* tests showed no significant differences between the two groups for both E and G.

by 4R tau fibrils and more efficient recruitment of 3R than 4R tau monomers by 3R tau fibrils, suggesting some degree of conformational mismatch between the two tau isoform types in fibril assembly (Nonaka et al., 2010; Dinkel et al., 2011; Furukawa et al., 2011). These experiments thus provide a possible explanation for the isoform-specific compositions of tau aggregates in CBD, PSP, and Pick's disease. As 4R tau seeds do not appear to effectively recruit 3R tau, it would seem that in AD, either a mixture of isoform-specific 3R and 4R tau fibrils are formed or initial 3R tau–nucleating structures recruit both 4R and 3R tau to yield a distinct type of hybrid fibrils that can seed both isoform types equally well thereafter (Dinkel et al., 2011). Our current study presents evidence that supports the latter scenario, as 4R and 3R tau appear to be interchangeable subunits of AD-tau, which can be incorporated into the same filament in a random, nonobligatory manner. This implies that AD PHFs display conformations that can be adopted by both 4R and 3R tau monomers during fibril assembly, thereby offering a parsimonious explanation for the unbiased recruitment of all six tau isoforms into NFTs. Interestingly, a recent paper that analyzed the trypsin-resistant core of tau aggregates isolated from different tauopathies identified the core structure of AD NFTs to consist of R2-R3-R4 MT-binding repeats from 4R tau and R1-R3-R4 from 3R tau (Taniguchi-Watanabe et al., 2016). The inclusion of only three MT-binding repeats from 4R tau in the fibril core would conceivably allow perfect alignment with the three MT-binding repeats from 3R tau, leading to flexible recruitment of either 4R or 3R tau into AD PHFs. In contrast, the core structures of 4R tau aggregates found in CBD and PSP were shown to span from R1 to R4 (Taniguchi-Watanabe et al., 2016), which would preclude easy alignment with 3R tau.

Notably, despite the abundance of tau inclusions developed in select brain regions interconnected with the primary site receiving AD-tau inoculum, the distribution of tau pathology is relatively circumscribed (see Fig. 6, A and B), which may indicate selective vulnerability of different brain regions to the development of tau aggregation and/or a limited transmission of tau pathology. In fact, only a small

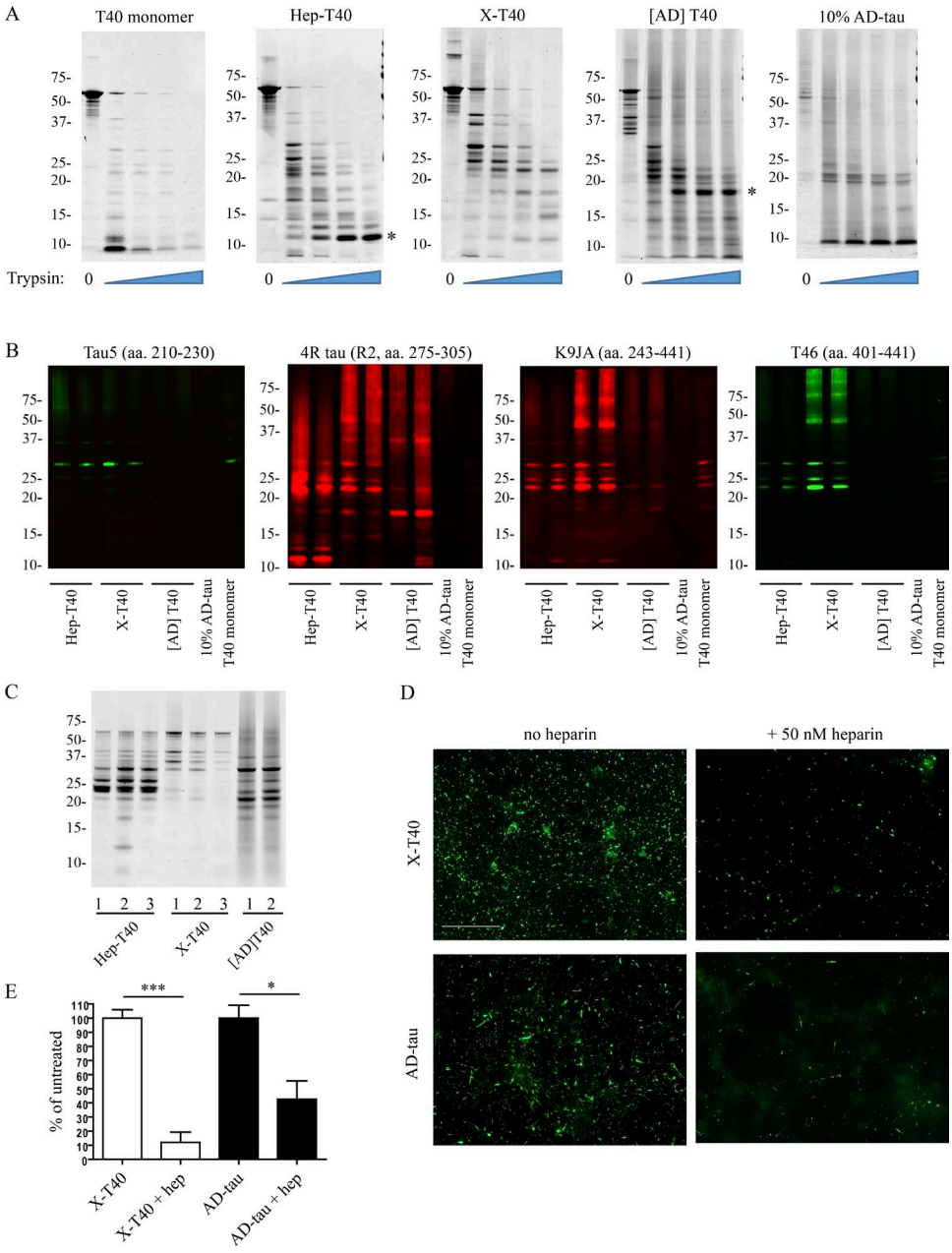

Figure 10. **The differential seeding activities of distinct tau fibril variants are underlain by their conformational differences and influenced by the presence of heparin.** (A) The different variants of tau fibrils (Hep-T40, X-T40, and [AD]T40) and control samples (equal amount of T40 monomer; 10% of AD-tau) were incubated with increasing concentrations of trypsin (0%, 0.00125%, 0.0025%, 0.005%, and 0.01%) for 30 min at 37°C. The resulted digestion products were resolved on SDS-PAGE and stained by Coomassie blue. The asterisk indicates dominant trypsin-resistant fragments for Hep-T40 and [AD]T40 fibrils. The 10% AD-tau seeds in [AD]T40 did not contribute to the 18-kD fragment, as suggested by the 10% AD-tau control. For each fibril variant, three to four independently prepared samples were tested across three independent experiments. (B) Digestion products from incubation with 0.01% trypsin were resolved on SDS-PAGE and immunoblotted with tau antibodies recognizing different epitopes. R2: second MT-binding repeat. Data are representative of three independent experiments. (C) The different variants of tau fibrils (three preparations of Hep-T40 fibrils, three preparations of X-T40 fibrils, and two preparations of [AD]T40 fibrils) were incubated with 1 µg/ml of proteinase K for 30 min at 37°C. The resulted products were resolved on SDS-PAGE and stained by Coomassie blue. (A–C) Molecular mass is indicated in kilodaltons. (D) Methanol-resistant mouse tau pathology induced by 1.5 µg X-T40 or 0.15 µg AD-tau fibrils with and without 50 nM heparin cotreatment. The amount of heparin added is equivalent to that contained in 10 µM heparin-induced 40 µM T40 fibrils added at 4.5 µg of tau per coverslip. Bar, 100 µm. (E) Quantification of mouse tau pathology for experiments shown in D. For each fibril variant, three different preparations of fibrils were tested across three independent sets of non-Tg neurons. Data are shown as mean + SEM. Pairwise Student's *t* tests were performed between untreated and heparin-treated cells. *, $P < 0.05$; ***, $P < 0.001$.

number of brain regions had newly emerged tau inclusions between 3 and 6 mo p.i., with no further spreading occurring from 6 to 9 mo p.i. These results suggest that, even with administration of the pathological tau conformers that plague AD brains, the self-amplification of tau aggregates alone is insufficient to fully recapitulate the extent of NFT progression observed in AD brains. We speculate that other factors may work in concert with pathological tau to sustain and continuously propagate lesions to wider networks in diseased human brains. As suggested by previous studies, the presence of Aβ plaques may enhance both the development and spreading of tau pathology (Götz et al., 2001; Lewis et al., 2001; Pooler et al., 2015). Interestingly, our study shows that the age of non-Tg mice inoculated with AD-tau has a modulatory effect on the spreading of tau pathology, conceivably because of slightly impaired protein quality control systems in aged mice. One can imagine an even more pronounced effect of aging in human brains, given the much longer lifespan of humans, consistent with aging being the greatest risk factor for AD and other neurodegenerative diseases. Importantly, our new paradigm of tau pathology induction, which no longer relies on tau Tg mice, would enable more convenient interrogation of factors modulating pathological tau transmission, using animals with different genetic modifications.

In summary, our study suggests that AD PHFs represent a unique conformational variant of tau fibrils that are distinct from synthetic tau fibrils, including the commonly used heparin-induced fibrils. The higher seeding potency of AD PHFs, coupled with our improved protocol of isolating large quantities of enriched PHFs, allowed us to demonstrate in vivo transmission of pathological tau in non-Tg mice, thus establishing a physiologically relevant mouse model of sporadic tauopathies amenable for mechanistic and therapeutic investigations.

MATERIALS AND METHODS

Animals

C57BL6, C57BL6/C3H F1, and CD1 mice were purchased from Charles River. 2–3-month-old C57BL6 and C57BL6/C3H F1 mice were used for intracerebral inoculation of different tau fibrils. 15–19-mo-old C57BL6 mice were also used for AD-tau injection. Embryos from pregnant CD1 mice were used to obtain primary hippocampal or cortical neurons. All animal care and experimental protocols were approved by the University of Pennsylvania's Institutional Animal Care and Use Committee.

Purification of Tau PHFs from AD brains

Human brain tissues from four sporadic AD patients, three Down syndrome patients with abundant tau pathology qualified for AD (referred to as AD/DS), and two normal controls were used in this study (Table S1). All cases used were histologically confirmed. Two of the AD/DS cases were provided by the University of Washington brain bank. The use of postmortem brain tissues for research was approved by the University of Pennsylvania's Institutional Review Board with informed consent from patients or their families. For each purification, 6–14 g of frontal cortical gray matter was homogenized using a Dounce homogenizer in nine volumes (v/w) of high-salt buffer (10 mM Tris-HCl, pH 7.4, 0.8 M NaCl, 1 mM EDTA, and 2 mM dithiothreitol [DTT], with protease inhibitor cocktail, phosphatase inhibitor, and PMSF) with 0.1% sarkosyl and 10% sucrose added and centrifuged at 10,000 *g* for 10 min at 4°C. Pellets were reextracted once or twice using the same buffer conditions as the starting materials, and the supernatants from all two to three initial extractions were filtered and pooled. Additional sarkosyl was added to the pooled low-speed supernatant to reach 1%. After 1-h nutation at room temperature, samples were centrifuged again at 300,000 *g* for 60 min at 4°C. The resulted 1% sarkosyl-insoluble pellets, which contain pathological tau, were washed once in PBS and then resuspended in PBS (~100 µl/g gray matter) by passing through 27-G 0.5-in. needles. The resuspended sarkosyl-insoluble pellets were further purified by a brief sonication (20 pulses at ~0.5 s/pulse) using a hand-held probe (QSonica) followed by centrifugation at 100,000 *g* for 30 min at 4°C, whereby the majority of protein contaminants were partitioned into the supernatant, with 60–70% of tau remaining in the pellet fraction. The pellets were resuspended in PBS at one fifth to one half of the precentrifugation volume, sonicated with 20–60 short pulses (~0.5 s/pulse), and spun at 10,000 *g* for 30 min at 4°C to remove large debris. The final supernatants, which contained enriched AD PHFs, were used in the study and referred to as AD-tau. In a subset of the experiments, the samples were boiled for 10 min right before the final 10,000-*g* spin to get rid of contaminating protease activity. The same purification protocol was used to prepare brain extracts from the two normal controls. The different fractions from PHF purification were characterized by Ponceau S staining, Western blotting (refer to Table S3 for antibodies), and sandwich ELISA for tau. The final supernatant fraction was further analyzed by transmission EM, BCA assay (Thermo Fisher Scientific), silver staining (SilverQuest Silver Staining kit; Thermo Fisher Scientific), and sandwich ELISA for Aβ 1–40, Aβ 1–42, and α-syn. The frontal cortex from one AD/DS case was purified using the traditional procedure with sucrose gradient fractionation as previously reported (Boluda et al., 2015). Enriched AD PHFs prepared using both methods showed similar seeding activity in primary hippocampal neurons from CD1 (non-Tg) mice.

Sandwich ELISA

The concentrations of tau, Aβ 1–40, and Aβ 1–42 in AD-tau preparations were measured using sandwich ELISA as previously described (Lee et al., 2003; Guo and Lee, 2011) with the following combinations of capture/reporting antibodies: Tau5/BT2 + HT7 for tau, Ban50/BA27 for Aβ 1–40, and Ban50/BC05 for Aβ 1–42. For measuring α-syn concentrations, a 384-well Maxisorp clear plate (Thermo Fisher Scientific) was coated with monoclonal antibody 9027 in Takeda buffer overnight at 4°C, washed, and blocked with

Block Ace solution (AbD Serotec) overnight at 4°C. AD-tau preparations were diluted at 1:100 for loading onto the plate with serially diluted recombinant α-syn monomers used as standards. After overnight incubation at 4°C, the plate was washed and incubated with monoclonal rabbit antibody MJF-R1 for overnight at 4°C. After washing and incubation with HRP-conjugated goat–anti–rabbit secondary antibody for 1 h at 37°C, the plate was developed using 1-Step Ultra TMB-ELISA Substrate solution (Thermo Fisher Scientific) for 10–15 min, quenched with 10% phosphoric acid, and read at 450 nm on a plate reader (M5; Spectramax).

Immunodepletion of tau from AD-tau preparations

Monoclonal anti-tau antibody Tau5 (IgG1) was covalently conjugated to Dynabeads (M-280 Tosylactivated; Thermo Fisher Scientific) per the manufacturer's instructions. Immunodepletion of tau was performed by incubating 200 µl of diluted AD-tau preparations containing 2 µg tau with Tau5/bead complex containing 20 µg Tau 5 overnight at 4°C with rotation. The unbound fraction was separated from the antibody/bead complex using a magnet, whereas the bound fraction was boiled with SDS sample buffer for 10 min to elute proteins from the beads. Mock immunodepletion was performed using a control mouse IgG1 antibody that does not recognize tau.

rTau purification and in vitro fibrillization

Different isoforms of rTau protein used in the study were expressed in BL21 (DE3) RIL cells and purified by cationic exchange using fast protein liquid chromatography as previously described (Li and Lee, 2006). For heparin-induced fibrillization, 40 µM recombinant T40 (4R2N tau) monomers were mixed with 10 µM or 40 µM low–molecular weight heparin and 2 mM DTT in Dulbecco's PBS (DPBS) without Ca^{2+} and Mg^{2+} (pH adjusted to 7; Cellgro; Corning) and incubated at 37°C for 5–7 d with constant agitation at 1,000 rpm. To minimize the amount of heparin added to neurons or injected into mice, fibrillization mixtures were centrifuged at 100,000 *g* for 30 min at 22°C with the resulting pellet resuspended into DPBS without heparin and DTT. Repetitive self-seeding of tau was conducted as previously described for α-syn (Guo et al., 2013). Cofactor-free de novo fibrillization of T40 was performed under the same conditions as heparin-induced fibrillization except for the exclusion of heparin from the reaction, and the resulting samples were termed passage 1 (P1). P2 reactions were set up at 40 µM total tau, with 90% fresh monomers and 10% tau from P1 that had been sonicated with a hand-held probe, and incubated at 37°C for 5–7 d with constant agitation at 1,000 rpm. This process was repeated for later passages. A sedimentation test was performed by centrifuging fibrillization products at 100,000 *g* for 30 min at 22°C, and equal volumes of supernatant and pellet fractions were analyzed on SDS-PAGE followed by Coomassie blue staining. Stained gels were scanned using an ODY-2816 imager (LI-COR Biosciences). Repetitive self-seeded fibrillization always led to the emergence of tau recovered in the pellet fraction at later passages, although the X-T40 variant that is seeding competent in non-Tg neurons was only stochastically generated in a subset of the self-seeding series.

In vitro phosphorylation of tau

The phosphorylation reaction was conducted by incubating 12 µM or 45 µM T40 with 1 U/ml stress-activated protein kinase 4 (SAPK4; EMD Millipore) overnight at 30°C in 25 mM Tris-HCl, pH 7.4, containing 0.1 mM EGTA, 10 mM magnesium acetate, 2 mM ATP, 1 mM PMSF, and protease inhibitor cocktail. The reaction was heat inactivated at 95°C for 5 min and centrifuged at 100,000 *g* for 15 min at 4°C. The supernatants, which contained phosphorylated tau, were transferred to new tubes for further experiments. Mock reaction was performed by treating T40 with the same conditions but without adding SAPK4.

In vitro fibrillization of rTau seeded by AD-tau

rTau at a total concentration of 9 or 36 µM was mixed with ∼1 or 4 µM AD-tau (calculated based on sandwich ELISA and the average molecular weight of all six tau isoforms), respectively, for 10% seeding and incubated in DPBS containing 2 mM DTT for 3–4 d at 37°C with constant agitation at 1,000 rpm. For cofibrillization of (Myc-) T40 and (HA-) T39 or fibrillization of all six isoforms of rTau, an equal molar concentration was used for each isoform in the reaction. For calculating percentage of pelletable tau formed as a result of seeding, percentage of pelletable tau from nonfibrillized monomer controls was subtracted in each set of experiments.

Transmission EM

Negative staining EM was performed as previously described (Guo and Lee, 2011) for the different variants of tau fibrils. For double-labeling immuno-EM, samples were absorbed onto carbon/formvar-coated copper grids for 5 min, washed three times for 5 min each by floating the grids on drops of PBS, and blocked for 5 min by floating on blocking buffer containing 10% BSA, 1% fish gelatin, and 0.02% sodium azide in PBS. The grids were then incubated with two primary antibodies for 1–2 h followed by three times of 5 min wash on PBS drops and 5 min on blocking buffer. After further incubation with anti–mouse and anti–rabbit secondary antibodies conjugated to 6 or 12 nm colloidal gold (Jackson ImmunoResearch Laboratories, Inc.) for 1–2 h, the grids were negatively stained using 1% uranyl acetate after three PBS washes and two distilled water washes. To rule out nonspecific binding of secondary antibodies, some experiments were performed with a single primary antibody but both secondary antibodies. All antibodies were diluted in blocking buffer. Antibody solutions, blocking buffer, and PBS wash solution were all filtered through 0.2-µm syringe filters before use. All EM pictures were taken with a Joel 1010 electron microscope.

Protease digestion of tau fibrils

Reactions were set up at 20 µl by mixing 6 µl of 40 µM tau fibrils with appropriate concentrations of trypsin or proteinase K, as indicated in the figure legends, in DPBS. After 30-min incubation at 37°C, samples were boiled with SDS sample buffer for 5 min (proteinase K reactions were stopped by 1 mM PMSF before sample buffer addition). Digestion products were then resolved on NuPAGE Novex 12% Bis-Tris gels (Invitrogen) and either stained with Coomassie blue solution or transferred to a nitrocellulose membrane for immunoblotting.

Primary neuron culture and fibril treatment

Primary neuron cultures were prepared from E16–E18 embryos from pregnant CD1 mice. Dissociated hippocampal or cortical tissues were digested with papain (Worthington Biochemical Corporation), triturated and strained into single neurons using a Falcon cell strainer (BD), and plated onto coverslips or plates precoated with poly-D-lysine (Sigma-Aldrich) diluted in borate buffer (0.05 M boric acid, pH 8.5) at 100,000 cells per coverslip on 24-well plates for immunocytochemistry or 375,000 cells per well on 12-well plates for biochemistry. Neurons were treated with tau fibrils that had been sonicated with 60 pulses by a hand-held probe on 6 or 7 d in vitro. The amount of tau added per coverslip/well is indicated in the figure legends. For the heparin inhibition experiment, 50 nM heparin was added to neurons together with tau fibrils. Immunocytochemistry or biochemical extraction was performed at 15 or 19 d after fibril treatment.

Immunocytochemistry

Neurons were fixed with prechilled methanol at −20°C for 15 min or with ice-cold 4% paraformaldehyde (PFA) containing 1% Triton X-100 at room temperature for 15 min to remove soluble tau. Normal tau staining was performed on neurons fixed with 4% PFA and permeabilized with 0.1% Triton X-100. After blocking with 3% BSA and 3% FBS for at least 1 h at room temperature, cells were incubated with specific primary antibodies (Table S3) overnight at 4°C followed by staining with appropriate Alexa Fluor 594– or 488–conjugated secondary antibodies (Invitrogen) for 2 h at room temperature. Coverslips were mounted using Fluoromount-G containing DAPI (SouthernBiotech) to label cell nuclei. Immunofluorescence images were acquired using a microscope (BX 51; Olympus) equipped with a digital camera (DP71) and DP manager (Olympus). For the quantification of the tau pathology shown in Fig. 2 B, Fig. 8 B, and Fig. 9 (E and G), whole coverslips were scanned using a Lamina Multilabel Slide scanner (PerkinElmer) and quantified using the image analysis platform HALO (Indica Laboratories). Quantification of the pathology shown in Fig. 8 E was performed on random-field images (10 images per condition) using ImageJ (National Institutes of Health).

Biochemical extraction of neurons and Western blotting

To investigate the expression profile of tau isoforms in cultured non-Tg neurons, cells were lysed with radioimmunoprecipitation assay (RIPA) buffer (50 mM Tris, pH 8.0, 150 mM NaCl, 1% NP-40, 5 mM EDTA, 0.5% sodium deoxycholate, and 0.1% SDS) containing protease inhibitor cocktail, sonicated, and centrifuged at 100,000 *g* for 30 min at 4°C with the supernatants saved for analysis. To confirm the induction of insoluble tau aggregates, neurons in 12-well plates were scraped into 1% sarkosyl lysis buffer (1% sarkosyl in 50 mM Tris and 150 mM NaCl, pH 7.6) containing protease inhibitor cocktail, sonicated, and centrifuged at 100,000 *g* for 30 min at 4°C. The supernatants were saved as the sarkosyl-soluble fraction, whereas pellets were resonicated in 1% sarkosyl lysis buffer and centrifuged again at 100,000 *g* for 30 min at 4°C. The resulted pellets were resuspended in DPBS at one third of the initial volume and sonicated to clear the solution and were saved as the sarkosyl-insoluble fraction. Protein concentrations in the RIPA extracts or sarkosyl-soluble fraction were determined using BCA assay. 10–20 µg of proteins from these fractions and an equal volume of corresponding insoluble fraction were loaded per lane on SDS-PAGE, transferred to nitrocellulose membranes, and blocked in Odyssey blocking buffer (LI-COR Biosciences) or 5% milk diluted in Tris-buffered saline before being immunoblotted with specific primary antibodies (Table S3). The blots were further incubated with IRDye-labeled secondary antibodies and scanned using an ODY-2816 imager. Dephosphorylation of RIPA extracts was performed by mixing 10 µg of total proteins with 1 µl of 400,000 U/ml of lambda protein phosphatase (New England Biolabs, Inc.) in 30 µl of reaction containing 1 mM $MnCl_2$ and 1× NEBuffer for MetalloPhosphatases and incubating for 3 h at 30°C.

Generation of mouse tau–specific polyclonal antibody

The polyclonal antibody R2295 was generated by immunizing rabbits with recombinant 4R2N mouse tau (Covance). The serum was first affinity purified against human tau by passing through an *N*-hydroxysuccinimide–activated agarose column (Thermo Fisher Scientific) coupled to recombinant 4R2N human tau. This process was performed twice, whereby the eluates were collected as the fraction of antibodies recognizing both human and mouse tau (Fig. 2, I and J), and the flow-through from the second pass was affinity purified using an *N*-hydroxysuccinimide–activated agarose column coupled to recombinant 4R2N mouse tau. The eluates from the mouse tau–coupled column were verified to be specific to mouse tau by Western blotting of rTau and immunostaining of cells expressing mouse or human tau.

Stereotaxic surgery on non-Tg mice

2–3-mo-old C57BL6 or C57BL6/C3H F1 mice or 15–19-mo-old C57BL6 mice were deeply anesthetized with ketamine/xylazine/acepromazine and immobilized in a stereotaxic frame (David Kopf Instruments) installed with both a stereotaxic robot and a microinjection robot (Neurostar) for motorized, computer-controlled injections. Animals were aseptically inoculated with synthetic tau fibrils or human

brain extracts in the dorsal hippocampus and overlying cortex of one hemisphere (bregma: −2.5 mm; lateral: 2 mm; depth: −2.4 mm and −1.4 mm from the skull) using a Hamilton syringe. Each of the two injection sites received 2.5 µl of inoculum, with the synthetic tau fibrils (both Hep-T40 and X-T40 fibrils) prepared at 1.8 µg tau/µl (4.5 µg tau/site) and AD-tau prepared at 1.6 µg tau/µl (4 µg tau/site) or 0.4 µg tau/µl (1 µg tau/site). Materials were injected into the hippocampus first (−2.4 mm from the skull) before the needle was pulled vertically upwards to the cortical injection site (−1.4 mm from the skull). We noted that the majority of the injected materials were deposited at the dorsal hilus of the hippocampus (see Fig. 5, A and B). The number and strain of mice used for each experimental condition are summarized in Table S4.

Histology and immunohistochemistry (IHC)

Inoculated mice were sacrificed and analyzed as previously described (Iba et al., 2013). In brief, animals were perfused at different time points after stereotaxic surgery (summarized in Table S4). Their brains were fixed in formalin, embedded in paraffin, and sectioned into 6-µm thickness. After deparaffinization and rehydration, the brain sections were immunostained with different antibodies (Table S3) and developed using a polymer horseradish peroxidase detection system (Biogenex) with hematoxylin counterstaining. ThS and AT8 double-labeling immunofluorescence was conducted to visualize mature tangle-like tau inclusions as follows: slides were stained with 0.0125% ThS, differentiated in 50% ethanol/50% PBS for 30 min, and incubated overnight with AT8 for immunofluorescence; the slides were dipped in Sudan black for 1 min before mounting to reduce autofluorescence. For quantification of the tau pathology shown in Fig. 3 F and Fig. 4 (B and E–G) as well as neuronal counts shown in Fig. 3 G and Fig. 4 C, two to three brain sections containing the region of interest were selected from each mouse, stained with AT8 for tau pathology or with an anti-NeuN antibody for neuronal count, scanned using a Lamina Multilabel Slide scanner, and quantified using the image analysis platform HALO. Semiquantitative analyses on the distribution of tau pathology induced by 8-µg AD-tau/mouse injection were performed as previously described (Iba et al., 2013), whereby the extent of AT8-positive pathology induced at 3 and 6 mo p.i. was examined for every 20th of coronal sections and graded as 0–3 (0: no pathology; 3: high pathology) for six coronal sections (Bregma 0.98, −2.18, −2.92, −3.52, −4.96, and −5.52 mm) that capture all affected brain structures. Averaged scores from the four mice at each time point were imported into a customized software to create heat maps of pathology distribution (Fig. 6 A).

Statistical analyses

For data shown in Fig. 3 (F and G) and Fig 4 (B and C), one-way ANOVA was performed with Tukey's posthoc test. For all the other statistical analyses, two-tailed unpaired Student's *t* tests were conducted for selected comparisons described in the figure legends. Differences with p-values <0.05 are considered significant.

Online supplemental material

Table S1 shows the demographics of human cases used in the study. Table S2 shows characterization of the final supernatant fraction from human brain extractions. Table S3 shows the antibodies used in this study. Table S4 shows a summary of inoculated mice analyzed for IHC.

ACKNOWLEDGMENTS

We thank L. Kwong, S. Boluda, J. Robinson, T. Schuck, J. Daniels, B. Zoll, D. Riddle, M. Byrne, A. Yousef, and J. Durante for advice or technical assistance, K. Brunden, K. Luk, and E. Lee for critical reading of the manuscript, L. Binder for providing Tau5, and P. Davies for contributing PHF-1, MC1, and TG3 antibodies. We also thank the patients and their families for brain donations and the University of Washington brain bank for providing additional brain samples.

This work was funded by the National Institutes of Health (grant nos. AG10124 and AG17586), CurePSP, and the Woods Foundation. J.L. Guo was supported by a postdoctoral fellowship award from Sophie M. Moyer and other donors of the AD research program of the BrightFocus Foundation (grant no. A2014005F).

The authors declare no competing financial interests.

Submitted: 3 June 2016
Accepted: 16 September 2016

REFERENCES

Adams, S.J., M.A. DeTure, M. McBride, D.W. Dickson, and L. Petrucelli. 2010. Three repeat isoforms of tau inhibit assembly of four repeat tau filaments. *PLoS One.* 5:e10810. http://dx.doi.org/10.1371/journal.pone.0010810

Boluda, S., M. Iba, B. Zhang, K.M. Raible, V.M. Lee, and J.Q. Trojanowski. 2015. Differential induction and spread of tau pathology in young PS19 tau transgenic mice following intracerebral injections of pathological tau from Alzheimer's disease or corticobasal degeneration brains. *Acta Neuropathol.* 129:221–237. http://dx.doi.org/10.1007/s00401-014-1373-0

Chirita, C.N., M. Necula, and J. Kuret. 2003. Anionic micelles and vesicles induce tau fibrillization *in vitro*. *J. Biol. Chem.* 278:25644–25650. http://dx.doi.org/10.1074/jbc.M301663200

Clavaguera, F., T. Bolmont, R.A. Crowther, D. Abramowski, S. Frank, A. Probst, G. Fraser, A.K. Stalder, M. Beibel, M. Staufenbiel, et al. 2009. Transmission and spreading of tauopathy in transgenic mouse brain. *Nat. Cell Biol.* 11:909–913. http://dx.doi.org/10.1038/ncb1901

Clavaguera, F., H. Akatsu, G. Fraser, R.A. Crowther, S. Frank, J. Hench, A. Probst, D.T. Winkler, J. Reichwald, M. Staufenbiel, et al. 2013. Brain homogenates from human tauopathies induce tau inclusions in mouse brain. *Proc. Natl. Acad. Sci. USA.* 110:9535–9540. http://dx.doi.org/10.1073/pnas.1301175110

Cleveland, D.W., S.Y. Hwo, and M.W. Kirschner. 1977a. Physical and chemical properties of purified tau factor and the role of tau in microtubule assembly. *J. Mol. Biol.* 116:227–247. http://dx.doi.org/10.1016/0022-2836(77)90214-5

Cleveland, D.W., S.Y. Hwo, and M.W. Kirschner. 1977b. Purification of tau, a microtubule-associated protein that induces assembly of microtubules from purified tubulin. *J. Mol. Biol.* 116:207–225. http://dx.doi.org/10.1016/0022-2836(77)90213-3

Colby, D.W., and S.B. Prusiner. 2011. De novo generation of prion strains. *Nat. Rev. Microbiol.* 9:771–777. http://dx.doi.org/10.1038/nrmicro2650

Dinkel, P.D., A. Siddiqua, H. Huynh, M. Shah, and M. Margittai. 2011. Variations in filament conformation dictate seeding barrier between

three- and four-repeat tau. *Biochemistry.* 50:4330–4336. http://dx.doi.org/10.1021/bi2004685

Espinoza, M., R. de Silva, D.W. Dickson, and P. Davies. 2008. Differential incorporation of tau isoforms in Alzheimer's disease. *J. Alzheimers Dis.* 14:1–16.

Falcon, B., A. Cavallini, R. Angers, S. Glover, T.K. Murray, L. Barnham, S. Jackson, M.J. O'Neill, A.M. Isaacs, M.L. Hutton, et al. 2015. Conformation determines the seeding potencies of native and recombinant Tau aggregates. *J. Biol. Chem.* 290:1049–1065. http://dx.doi.org/10.1074/jbc.M114.589309

Friedhoff, P., M. von Bergen, E.M. Mandelkow, P. Davies, and E. Mandelkow. 1998. A nucleated assembly mechanism of Alzheimer paired helical filaments. *Proc. Natl. Acad. Sci. USA.* 95:15712–15717. http://dx.doi.org/10.1073/pnas.95.26.15712

Frost, B., R.L. Jacks, and M.I. Diamond. 2009. Propagation of tau misfolding from the outside to the inside of a cell. *J. Biol. Chem.* 284:12845–12852. http://dx.doi.org/10.1074/jbc.M808759200

Furukawa, Y., K. Kaneko, and N. Nukina. 2011. Tau protein assembles into isoform- and disulfide-dependent polymorphic fibrils with distinct structural properties. *J. Biol. Chem.* 286:27236–27246. http://dx.doi.org/10.1074/jbc.M111.248963

Goedert, M., M.G. Spillantini, R. Jakes, D. Rutherford, and R.A. Crowther. 1989. Multiple isoforms of human microtubule-associated protein tau: sequences and localization in neurofibrillary tangles of Alzheimer's disease. *Neuron.* 3:519–526. http://dx.doi.org/10.1016/0896-6273(89)90210-9

Goedert, M., R. Jakes, M.G. Spillantini, M. Hasegawa, M.J. Smith, and R.A. Crowther. 1996. Assembly of microtubule-associated protein tau into Alzheimer-like filaments induced by sulphated glycosaminoglycans. *Nature.* 383:550–553. http://dx.doi.org/10.1038/383550a0

Götz, J., F. Chen, J. van Dorpe, and R.M. Nitsch. 2001. Formation of neurofibrillary tangles in P301l tau transgenic mice induced by Aβ42 fibrils. *Science.* 293:1491–1495. http://dx.doi.org/10.1126/science.1062097

Guo, J.L., and V.M.Y. Lee. 2011. Seeding of normal Tau by pathological Tau conformers drives pathogenesis of Alzheimer-like tangles. *J. Biol. Chem.* 286:15317–15331. http://dx.doi.org/10.1074/jbc.M110.209296

Guo, J.L., and V.M.Y. Lee. 2013. Neurofibrillary tangle-like tau pathology induced by synthetic tau fibrils in primary neurons over-expressing mutant tau. *FEBS Lett.* 587:717–723. http://dx.doi.org/10.1016/j.febslet.2013.01.051

Guo, J.L., and V.M.Y. Lee. 2014. Cell-to-cell transmission of pathogenic proteins in neurodegenerative diseases. *Nat. Med.* 20:130–138. http://dx.doi.org/10.1038/nm.3457

Guo, J.L., D.J. Covell, J.P. Daniels, M. Iba, A. Stieber, B. Zhang, D.M. Riddle, L.K. Kwong, Y. Xu, J.Q. Trojanowski, and V.M. Lee. 2013. Distinct α-synuclein strains differentially promote tau inclusions in neurons. *Cell.* 154:103–117. http://dx.doi.org/10.1016/j.cell.2013.05.057

Holmes, B.B., S.L. DeVos, N. Kfoury, M. Li, R. Jacks, K. Yanamandra, M.O. Ouidja, F.M. Brodsky, J. Marasa, D.P. Bagchi, et al. 2013. Heparan sulfate proteoglycans mediate internalization and propagation of specific proteopathic seeds. *Proc. Natl. Acad. Sci. USA.* 110:E3138–E3147. http://dx.doi.org/10.1073/pnas.1301440110

Iba, M., J.L. Guo, J.D. McBride, B. Zhang, J.Q. Trojanowski, and V.M. Lee. 2013. Synthetic tau fibrils mediate transmission of neurofibrillary tangles in a transgenic mouse model of Alzheimer's-like tauopathy. *J. Neurosci.* 33:1024–1037. http://dx.doi.org/10.1523/JNEUROSCI.2642-12.2013

Iba, M., J.D. McBride, J.L. Guo, B. Zhang, J.Q. Trojanowski, and V.M. Lee. 2015. Tau pathology spread in PS19 tau transgenic mice following locus coeruleus (LC) injections of synthetic tau fibrils is determined by the LC's afferent and efferent connections. *Acta Neuropathol.* 130:349–362. http://dx.doi.org/10.1007/s00401-015-1458-4

Kampers, T., P. Friedhoff, J. Biernat, E.M. Mandelkow, and E. Mandelkow. 1996. RNA stimulates aggregation of microtubule-associated protein tau into Alzheimer-like paired helical filaments. *FEBS Lett.* 399:344–349. http://dx.doi.org/10.1016/S0014-5793(96)01386-5

Kfoury, N., B.B. Holmes, H. Jiang, D.M. Holtzman, and M.I. Diamond. 2012. Trans-cellular propagation of Tau aggregation by fibrillar species. *J. Biol. Chem.* 287:19440–19451. http://dx.doi.org/10.1074/jbc.M112.346072

Lasagna-Reeves, C.A., D.L. Castillo-Carranza, U. Sengupta, M.J. Guerrero-Munoz, T. Kiritoshi, V. Neugebauer, G.R. Jackson, and R. Kayed. 2012. Alzheimer brain-derived tau oligomers propagate pathology from endogenous tau. *Sci. Rep.* 2:700. http://dx.doi.org/10.1038/srep00700

Lee, E.B., D.M. Skovronsky, F. Abtahian, R.W. Doms, and V.M. Lee. 2003. Secretion and intracellular generation of truncated Aβ in β-site amyloid-β precursor protein-cleaving enzyme expressing human neurons. *J. Biol. Chem.* 278:4458–4466. http://dx.doi.org/10.1074/jbc.M210105200

Lee, V.M., B.J. Balin, L. Otvos Jr., and J.Q. Trojanowski. 1991. A68: a major subunit of paired helical filaments and derivatized forms of normal Tau. *Science.* 251:675–678. http://dx.doi.org/10.1126/science.1899488

Lee, V.M., J. Wang, and J.Q. Trojanowski. 1999. Purification of paired helical filament tau and normal tau from human brain tissue. *Methods Enzymol.* 309:81–89. http://dx.doi.org/10.1016/S0076-6879(99)09008-4

Lee, V.M., M. Goedert, and J.Q. Trojanowski. 2001. Neurodegenerative tauopathies. *Annu. Rev. Neurosci.* 24:1121–1159. http://dx.doi.org/10.1146/annurev.neuro.24.1.1121

Lewis, J., D.W. Dickson, W.L. Lin, L. Chisholm, A. Corral, G. Jones, S.H. Yen, N. Sahara, L. Skipper, D. Yager, et al. 2001. Enhanced neurofibrillary degeneration in transgenic mice expressing mutant tau and APP. *Science.* 293:1487–1491. http://dx.doi.org/10.1126/science.1058189

Li, W., and V.M. Lee. 2006. Characterization of two VQIXXK motifs for tau fibrillization in vitro. *Biochemistry.* 45:15692–15701. http://dx.doi.org/10.1021/bi061422+

Luk, K.C., V. Kehm, J. Carroll, B. Zhang, P. O'Brien, J.Q. Trojanowski, and V.M. Lee. 2012a. Pathological α-synuclein transmission initiates Parkinson-like neurodegeneration in nontransgenic mice. *Science.* 338:949–953. http://dx.doi.org/10.1126/science.1227157

Luk, K.C., V.M. Kehm, B. Zhang, P. O'Brien, J.Q. Trojanowski, and V.M. Lee. 2012b. Intracerebral inoculation of pathological α-synuclein initiates a rapidly progressive neurodegenerative α-synucleinopathy in mice. *J. Exp. Med.* 209:975–986. http://dx.doi.org/10.1084/jem.20112457

Mandelkow, E., M. von Bergen, J. Biernat, and E.M. Mandelkow. 2007. Structural principles of tau and the paired helical filaments of Alzheimer's disease. *Brain Pathol.* 17:83–90. http://dx.doi.org/10.1111/j.1750-3639.2007.00053.x

Martin, L., X. Latypova, and F. Terro. 2011. Post-translational modifications of tau protein: implications for Alzheimer's disease. *Neurochem. Int.* 58:458–471. http://dx.doi.org/10.1016/j.neuint.2010.12.023

Masuda-Suzukake, M., T. Nonaka, M. Hosokawa, T. Oikawa, T. Arai, H. Akiyama, D.M. Mann, and M. Hasegawa. 2013. Prion-like spreading of pathological α-synuclein in brain. *Brain.* 136:1128–1138. http://dx.doi.org/10.1093/brain/awt037

Morozova, O.A., Z.M. March, A.S. Robinson, and D.W. Colby. 2013. Conformational features of tau fibrils from Alzheimer's disease brain are faithfully propagated by unmodified recombinant protein. *Biochemistry.* 52:6960–6967. http://dx.doi.org/10.1021/bi400866w

Nonaka, T., S.T. Watanabe, T. Iwatsubo, and M. Hasegawa. 2010. Seeded aggregation and toxicity of α-synuclein and tau: cellular models of neurodegenerative diseases. *J. Biol. Chem.* 285:34885–34898. http://dx.doi.org/10.1074/jbc.M110.148460

Oh, S.W., J.A. Harris, L. Ng, B. Winslow, N. Cain, S. Mihalas, Q. Wang, C. Lau, L. Kuan, A.M. Henry, et al. 2014. A mesoscale connectome of the mouse brain. *Nature.* 508:207–214. http://dx.doi.org/10.1038/nature13186

Paumier, K.L., K.C. Luk, F.P. Manfredsson, N.M. Kanaan, J.W. Lipton, T.J. Collier, K. Steece-Collier, C.J. Kemp, S. Celano, E. Schulz, et al. 2015. Intrastriatal injection of pre-formed mouse α-synuclein fibrils into rats triggers α-synuclein pathology and bilateral nigrostriatal degeneration. *Neurobiol. Dis.* 82:185–199. http://dx.doi.org/10.1016/j.nbd.2015.06.003

Peelaerts, W., L. Bousset, A. Van der Perren, A. Moskalyuk, R. Pulizzi, M. Giugliano, C. Van den Haute, R. Melki, and V. Baekelandt. 2015. α-Synuclein strains cause distinct synucleinopathies after local and systemic administration. *Nature.* 522:340–344. http://dx.doi.org/10.1038/nature14547

Peeraer, E., A. Bottelbergs, K. Van Kolen, I.C. Stancu, B. Vasconcelos, M. Mahieu, H. Duytschaever, L. Ver Donck, A. Torremans, E. Sluydts, et al. 2015. Intracerebral injection of preformed synthetic tau fibrils initiates widespread tauopathy and neuronal loss in the brains of tau transgenic mice. *Neurobiol. Dis.* 73:83–95. http://dx.doi.org/10.1016/j.nbd.2014.08.032

Petkova, A.T., R.D. Leapman, Z. Guo, W.M. Yau, M.P. Mattson, and R. Tycko. 2005. Self-propagating, molecular-level polymorphism in Alzheimer's β-amyloid fibrils. *Science.* 307:262–265. http://dx.doi.org/10.1126/science.1105850

Pooler, A.M., M. Polydoro, E.A. Maury, S.B. Nicholls, S.M. Reddy, S. Wegmann, C. William, L. Saqran, O. Cagsal-Getkin, R. Pitstick, et al. 2015. Amyloid accelerates tau propagation and toxicity in a model of early Alzheimer's disease. *Acta Neuropathol. Commun.* 3:14. http://dx.doi.org/10.1186/s40478-015-0199-x

Sanders, D.W., S.K. Kaufman, S.L. DeVos, A.M. Sharma, H. Mirbaha, A. Li, S.J. Barker, A.C. Foley, J.R. Thorpe, L.C. Serpell, et al. 2014. Distinct tau prion strains propagate in cells and mice and define different tauopathies. *Neuron.* 82:1271–1288. http://dx.doi.org/10.1016/j.neuron.2014.04.047

Siddiqua, A., and M. Margittai. 2010. Three- and four-repeat Tau coassemble into heterogeneous filaments: an implication for Alzheimer disease. *J. Biol. Chem.* 285:37920–37926. http://dx.doi.org/10.1074/jbc.M110.185728

Siddiqua, A., Y. Luo, V. Meyer, M.A. Swanson, X. Yu, G. Wei, J. Zheng, G.R. Eaton, B. Ma, R. Nussinov, et al. 2012. Conformational basis for asymmetric seeding barrier in filaments of three- and four-repeat tau. *J. Am. Chem. Soc.* 134:10271–10278. http://dx.doi.org/10.1021/ja303498q

Stancu, I.C., B. Vasconcelos, L. Ris, P. Wang, A. Villers, E. Peeraer, A. Buist, D. Terwel, P. Baatsen, T. Oyelami, et al. 2015. Templated misfolding of Tau by prion-like seeding along neuronal connections impairs neuronal network function and associated behavioral outcomes in Tau transgenic mice. *Acta Neuropathol.* 129:875–894. http://dx.doi.org/10.1007/s00401-015-1413-4

Stöhr, J., J.C. Watts, Z.L. Mensinger, A. Oehler, S.K. Grillo, S.J. DeArmond, S.B. Prusiner, and K. Giles. 2012. Purified and synthetic Alzheimer's amyloid beta (Aβ) prions. *Proc. Natl. Acad. Sci. USA.* 109:11025–11030. http://dx.doi.org/10.1073/pnas.1206555109

Taniguchi-Watanabe, S., T. Arai, F. Kametani, T. Nonaka, M. Masuda-Suzukake, A. Tarutani, S. Murayama, Y. Saito, K. Arima, M. Yoshida, et al. 2016. Biochemical classification of tauopathies by immunoblot, protein sequence and mass spectrometric analyses of sarkosyl-insoluble and trypsin-resistant tau. *Acta Neuropathol.* 131:267–280. http://dx.doi.org/10.1007/s00401-015-1503-3

von Bergen, M., S. Barghorn, S.A. Müller, M. Pickhardt, J. Biernat, E.M. Mandelkow, P. Davies, U. Aebi, and E. Mandelkow. 2006. The core of tau-paired helical filaments studied by scanning transmission electron microscopy and limited proteolysis. *Biochemistry.* 45:6446–6457. http://dx.doi.org/10.1021/bi052530j

Walker, L.C., and M. Jucker. 2015. Neurodegenerative diseases: expanding the prion concept. *Annu. Rev. Neurosci.* 38:87–103. http://dx.doi.org/10.1146/annurev-neuro-071714-033828

Weingarten, M.D., A.H. Lockwood, S.Y. Hwo, and M.W. Kirschner. 1975. A protein factor essential for microtubule assembly. *Proc. Natl. Acad. Sci. USA.* 72:1858–1862. http://dx.doi.org/10.1073/pnas.72.5.1858

Weissmann, C., M. Enari, P.C. Klöhn, D. Rossi, and E. Flechsig. 2002. Transmission of prions. *J. Infect. Dis.* 186:S157–S165. http://dx.doi.org/10.1086/344575

Wu, J.W., M. Herman, L. Liu, S. Simoes, C.M. Acker, H. Figueroa, J.I. Steinberg, M. Margittai, R. Kayed, C. Zurzolo, et al. 2013. Small misfolded Tau species are internalized via bulk endocytosis and anterogradely and retrogradely transported in neurons. *J. Biol. Chem.* 288:1856–1870. http://dx.doi.org/10.1074/jbc.M112.394528

Zhu, H.L., C. Fernández, J.B. Fan, F. Shewmaker, J. Chen, A.P. Minton, and Y. Liang. 2010. Quantitative characterization of heparin binding to Tau protein: implication for inducer-mediated Tau filament formation. *J. Biol. Chem.* 285:3592–3599. http://dx.doi.org/10.1074/jbc.M109.035691